National Technical University of Athens
School of Chemical Engineering
Department of Materials Science and Engineering

Computational Study of Chlorine Production in a Bipolar Electrochemical Reactor for Ballast Water Treatment

Postgraduate Program: Computational Mechanics

Vassilis Theocharis

Supervisor : A. Karantonis
Assistant Professor N.T.U.A.

Physical Chemistry and Applied Electrochemistry Laboratory
Athens, July 2015

National Technical University of Athens
School of Chemical Engineering
Department of Materials Science and Engineering
Physical Chemistry and Applied Electrochemistry Laboratory

Computational Study of Chlorine Production in a Bipolar Electrochemical Reactor for Ballast Tank Water Treatment

POSTGRADUATE PROGRAM: COMPUTATIONAL MECHANICS

Vassilis Theocharis

Supervisor : A. Karantonis
Assistant Professor N.T.U.A.

It has been approved on 3rd July 2015 by the following committee members:

(Signature)	*(Signature)*	*(Signature)*
....	....	....
Antonis Karantonis	Andreas Boudouvis	Dimitris Goussis
Assistant Professor N.T.U.A.	Professor N.T.U.A.	Professor N.T.U.A.

(Signature)

....
Vassilis Theocharis
Chemical Engineer N.T.U.A
© 2015 – All rights reserved

National Technical University of Athens
School of Chemical Engineering
Department of Materials Science and Engineering
Physical Chemistry and Applied Electrochemistry Laboratory

Copyright ©–All rights reserved Vassilis Theocharis, 2015.

Copies of this thesis, either in full or in extracts and whether in hard or electronic copy, may be made only for nonprofit educational purposes. Any quotation from the thesis or use of any of the information contained in it must acknowledge this thesis as the source of the quotation or information.

Acknowledgments

Foremost, I would like to express my sincere gratitude to my supervisor Assistant Professor Antonis Karantonis for the continuous support of my Master thesis, for his patience, motivation, enthusiasm, and immense knowledge whilst allowing me to work in my own way.

A very special thanks goes out to ERMA FIRST ESK Engineering Solutions S.A for generously providing us with the small-scale electrochemical reactor and specifically to Dr. Dimitris Koutsaftis for providing me with advices and technical support.

I would also like to thank Professor Andreas Boudouvis, Dr. Eleni Koronaki and Dr. George Pashos of the Dpt. Process Analysis and Plant Design for their suggestions.

I thank my fellow lab-mates Eleni Andreou, Yannis Antonopoulos, Panos Stamatopoulos, Pavlos Xrissafidis and Faidon Giannopoulos for the endless days we were working together and for all the fun we have had in the last months.

I must also acknowledge my former supervisors Alexandra Baila and Marco Gruber who expressed trust in my skills and gave me the great opportunity to work under their guidance.

Last but not the least, I would like to thank my father Laoklis for supporting me even at that age!

Abstract

Ballast water is an important factor for the stability and proper propulsion of ships. Ships fill their tanks with water at the port of departure and eject it at the port of destination. The introduction of new microorganisms in the marine ecosystem of the port of destination constitutes a major ecological problem. One of the methods used for the disinfection of ballast water is the electrolysis of seawater for the production of chlorine by anodic oxidation of chlorides. The aim of the present study is the modeling of an electrochemical reactor used for the production of chlorine, by using the COMSOL Multiphysics software. The reactor consists of two feeder electrodes (anode and cathode) and a sequence of bipolar electrodes in a parallel configuration. The feed of seawater is considered to be continuous and the problem is solved under stationary conditions. On every bipolar electrode, three reactions are taking place, the production of chlorine, the production of oxygen and the production of hydrogen. More specifically:

- The oxidation of chloride ions to chlorine occurs at the anode.
- Chlorine is hydrolyzed to hypochlorous oxide in the aqueous solution.
- Hypochlorous oxide is dissociated to hypochlorous anions and protons.
- The electrolysis of water to oxygen occurs at the anode.
- The reduction of water to hydrogen occurs at the cathode.

The computational study is based on the solution of a current distribution problem with boundary conditions the electrochemical kinetics on the feeders and the bipolar electrodes. The geometric characteristics of the reactor and the operational conditions are considered as parameters.

Περιληψη

Το έρμα των πλοίων (Ballast Water), στην ναυσιπλοΐα, αποτελεί σημαντικό παράγοντα ευστάθειας και σωστής πρόωσης των πλοίων. Τα πλοία γεμίζουν τις δεξαμενές τους με νερό από το λιμάνι αναχώρησης (ή/και κατά την διάρκεια του ταξιδιού τους) και το απορρίπτουν στο λιμάνι προορισμού. Η εισαγωγή των θαλάσσιων μικροοργανισμών που περιέχονται στο έρμα και απορρίπτονται σε νέο θαλάσσιο οικοσύστημα αποτελεί ένα σημαντικό οικολογικό πρόβλημα. Μια από τις εν πλω μεθόδους επεξεργασίας του έρματος είναι η παραγωγή χλωρίου με ηλεκτρόλυση για την απολύμανση του.

Σκοπός της εργασίας είναι η μοντελοποίηση ηλεκτροχημικού αντιδραστήρα για την εν πλω απολύμανση του έρματος μέσω του εμπορικού λογισμικού COMSOL. Ο αντιδραστήρας αποτελείται από ηλεκτρόδια τροφοδοσίας και από μία συστοιχία διπολικών ηλεκτροδίων σε παράλληλη διάταξη. Η παροχή του έρματος στον αντιδραστήρα θεωρείται συνεχής ενώ οι συνθήκες εντός αυτού μόνιμες. Σε κάθε διπολικό ηλεκτρόδιο λαμβάνουν χώρα τρεις κύριες ηλεκτροχημικές αντιδράσεις, η παραγωγή αέριου χλωρίου ($\mathrm{Cl_2}$), η παραγωγή αέριου οξυγόνου ($\mathrm{O_2}$) και η παραγωγή αέριου υδρογόνου ($\mathrm{H_2}$). Ειδικότερα:

- Στην άνοδο λαμβάνεται υπόψη η αντίδραση οξείδωσης των ιόντων χλωρίου προς μοριακό χλώριο, σύμφωνα με τον τον μηχανισμό Volmer-Tafel.
- Το στοιχειακό χλώριο υδρολύεται προς υποχλωριώδες οξύ στο υδατικό διάλυμα.
- Το υποχλωριώδες οξύ διίσταται σε υποχλωριώδη ιόντα και πρωτόνια.
- Στην άνοδο πραγματοποιείται επίσης η ηλεκτρόλυση του νερού προς οξυγόνο.
- Στην κάθοδο λαμβάνεται υπόψη η αναγωγή του νερού προς υδρογόνο.

Η υπολογιστική μελέτη βασίζεται στην λύση ενός προβλήματος κατανομής του ρεύματος, με συνοριακές συνθήκες, τόσο στα ηλεκτρόδια τροφοδοσίας όσο και στα διπολικά ηλεκτρόδια, τις κατάλληλες ηλεκτροκινητικές εξισώσεις που περιγράφουν τις ηλεκτροχημικές αντιδράσεις σε αυτά. Ως παράμετροι του προβλήματος θεωρούνται οι συνθήκες λειτουργίας και η γεωμετρία του αντιδραστήρα.

Contents

Acknowledgments i

Abstract iii

Περιληψη v

Contents vii

List of Figures ix

List of Tables xiii

1 Introduction 1
- 1.1 Generalities . . . 1
- 1.2 Electrode Materials . . . 3
- 1.3 Chlorine Evolution Reaction . . . 4
- 1.4 Oxygen Evolution Reaction . . . 8
- 1.5 Bipolar Electrodes . . . 9

2 Reactions Kinetics 11
- 2.1 Kinetics of Chlorine Evolution Reaction . . . 11
- 2.2 Kinetics of Oxygen Evolution Reaction . . . 14
- 2.3 Reactions in Homogeneous Phase . . . 18

3 Mathematical Formulation 21
- 3.1 Multi-Ion Transport in Dilute Electrolyte Solutions . . . 21
- 3.2 Poisson Equation . . . 23
- 3.3 Electroneutrality condition . . . 24
- 3.4 Charge Conservation . . . 24
- 3.5 Incompressible Flow . . . 25
  - 3.5.1 Laminar Flow . . . 26
  - 3.5.2 Turbulent Flow . . . 26

3.6 Mathematical Models 28
3.6.1 Secondary Current Distribution 28
3.6.2 Tertiary Current Distribution 29

4 Computational Approach 31
4.1 Geometry I 35
4.2 Geometry II 39
4.3 Geometry III 42
4.4 Geometry I with Secondary and Tertiary Models 45
4.5 Geometry I with Laminar and Turbulent Flow 52
4.6 Geometry I with Reaction Rates in Homogeneous Phase . . . 56
4.7 Complete Reactor 61

5 Conclusions 67

A Multiple steps reaction rate 69

List of Figures

1.1 *Small-scale electrochemical reactor implementing electrolysis for chlorine production.* . . . 3

1.2 *Polarization of bipolar electrodes during reactor operation.* . . . 3

1.3 *Model for surface oxidation of Pt: transition from OH monolayer, through rearranged OH/Pt state, to O/Pt-PtO structure.* . . . 7

2.1 *Relative distribution of main aqueous chlorine species as a function of pH at 25 ^oC and for a chloride concentration of $5 \cdot 10^{-3}$ M.* . . . 19

4.1 *Geometry I with four feeder electrodes (anode on the left and cathode on the right) and two bipolar electrodes (in the middle). Blue axis denotes symmetry plane* . . . 35

4.2 *Unstructured triangular mesh with boundary layer quadrilateral elements.* 35

4.3 *Velocity magnitude distribution of Geometry I.* . . . 36

4.4 *Applied potential 10 V in Geometry I:* ***a)*** *Electrolyte potential distribution and* ***b)*** *Electrolyte current density vector, y-component.* . . . 36

4.5 *Applied potential 10 V in Geometry I on the upper horizontal side of bipolar electrode:* ***a)*** *Local current density of the reactions producing Cl_2, O_2 and H_2 also the normal vector of electrolyte current density is plotted and* ***b)****Overpotential of the aforementioned reactions.* . . . 37

4.6 *Electrolyte current density vector, y-component of Geometry I for applied potential 30 V.* . . . 38

4.7 *Applied potential 30 V in Geometry I on the upper horizontal side of bipolar electrode:* ***a)*** *Local current density of the reactions producing Cl_2, O_2 and H_2 also the normal vector of electrolyte current density is plotted and* ***b)****Overpotential of the aforementioned reactions.* . . . 38

4.8 *Geometry II with four feeder electrodes (anode on the left and cathode on the right) and two bipolar electrodes (in the middle). Blue axis denotes symmetry plane* . . . 39

4.9 *Velocity magnitude distribution of Geometry II.* . . . 39

4.10 *Applied potential 10 V in Geometry II:* ***a)*** *Electrolyte potential distribution and* ***b)*** *Electrolyte current density vector, y-component.* 40
4.11 *Applied potential 10 V in Geometry II on the upper horizontal side of bipolar electrode:* ***a)*** *Local current density of the reactions producing Cl_2, O_2 and H_2 also the normal vector of electrolyte current density is plotted and* ***b)****Overpotential of the aforementioned reactions.* 41
4.12 *Chlorine Cl_2 concentration (mol/m_3) in the outlet of the reactor of Geometry I and Geometry II* 41
4.13 *Geometry III with four feeder electrodes (anode on the left and cathode on the right) and two bipolar electrodes (in the middle). Blue axis denotes symmetry plane* 42
4.14 *Velocity magnitude distribution of Geometry III.* 43
4.15 *Applied 10 V in Geometry III:* ***a)*** *Electrolyte potential distribution and* ***b)*** *Electrolyte current density vector, y-component.* 43
4.16 *Applied 10 V in Geometry III on the upper horizontal side of bipolar electrode:* ***a)*** *Local current density of the reactions producing Cl_2, O_2 and H_2 also the normal vector of electrolyte current density is plotted and* ***b)****Overpotential of the aforementioned reactions.* 44
4.17 *Chlorine Cl_2 concentration (mol/m_3) in the outlet of the reactor of Geometry I, Geometry II and Geometry III* 44
4.18 *Applied 10 V in Geometry III with Tertiary model:* ***a)*** *Electrolyte potential distribution in Tertiary model and* ***b)*** *Electrolyte potential along the reactor (at height of 0.006 m) for both Secondary and Tertiary models.* . 46
4.19 *Comparison of calculated normal electrolyte current density on the upper side of electrodes between Secondary and Tertiary models for applied* 10*V in Geometry I:* ***a)*** *Anode feeder electrode,* ***b)*** *Bipolar electrode and* ***c)*** *Cathode feeder electrode.* 47
4.20 *Applied 10 V in Geometry I, anode's concentrations of* ***a)*** *Chlorine (Cl_2) and* ***b)*** *Chloride ion (Cl^-) are depicted between both Secondary and Tertiary model.* 48
4.21 *Comparison of the concentration distribution, of the produced species Cl_2, OH^- and H^+, along the reactor (at height of 0.006 m) between the two models.* 49
4.22 *Deviation from electroneutrality condition of the Secondary model.* . . . 49
4.23 *Percentage error below 1% of the calculated Tertiary's electrolyte conductivity over the constant value of the Secondary model in the vicinity of* ***a)*** *anode and* ***b)*** *cathode.* 50
4.24 *Comparison of Norm Electrolyte current density, along the reactor (at height of 0.006 m), between the two models.* 51
4.25 *Velocity magnitude distribution of Turbulent module.* 52

4.26 *Applied voltage 30 V in Geometry I, comparison of:* ***a)*** *Electrolyte potential distribution and* ***b)*** *Norm electrolyte current density between cases with laminar (inlet velocity 0.05m/s) and turbulent flow (inlet velocity 1.5 m/s).* . . . 53
4.27 *Concentration distribution, of the produced species* Cl_2, OH^- *and* H^+, *along the reactor (at height of 0.006 m) between the cases of laminar (inlet velocity 0.05 m/s) and turbulent flow (inlet velocity 1.5 m/s).* . . . 53
4.28 *Concentrations of the produced Chlorine* Cl_2 *and Hydrogen ion* H^+ *are shown on* ***a), b)*** *Anode feeder electrode and* ***c), d)*** *Bipolar electrode for the laminar (inlet velocity 0.05 m/s) and turbulent flow (inlet velocity 1.5 m/s).* . . . 54
4.29 *Comparison of normal electrolyte current density between Laminar and Turbulent flow on the upper side of* ***a)*** *Anode feeder electrode,* ***b)*** *Bipolar electrode and* ***c)*** *Cathode feeder electrode.* . . . 55
4.30 *Comparison of* ***a)*** *Electrolyte potential and* ***b)*** *Norm electrolyte current density between the case without and with reaction rates in homogeneous phase (electrolyte).* . . . 57
4.31 *Comparison of normal electrolyte current density between the cases without and with reaction rates in homogeneous phase (electrolyte) on the upper side of* ***a)*** *Anode feeder electrode,* ***b)*** *Bipolar electrode and* ***c)*** *Cathode feeder electrode.* . . . 58
4.32 *Forward and backward rates of the* ***a)*** *Dissociation of water* (H_2O) *and* ***b)*** *Dissociation of hypochlorous acid (HOCl).* . . . 59
4.33 *Distribution of pH inside the reactor with Geometry I under implementation of reaction rates in the homogeneous phase of electrolyte.* . . . 60
4.34 *Concentration of chlorine* (Cl_2), *hypochlorous acid (HOCl) and hypochlorous anion* (OCl^-) *along the reactor (at height of 0.006 m).* . . . 60
4.35 *Concentration of chlorine* (Cl_2), *hypochlorous acid (HOCl) and hypochlorous anion* (OCl^-) *at the outlet of the reactor.* . . . 61
4.36 *Reactor with 2 anode feeder electrodes, 3 cathode feeder electrodes and 5 bipolar electrodes. Blue axis denotes symmetry plane.* . . . 61
4.37 *Velocity magnitude distribution of the complete reactor.* . . . 62
4.38 *Applied voltage 30 V in a full reactor with turbulent flow :* ***a)*** *Electrolyte potential distribution and* ***b)****Electrolyte current density vector, y-component.* 63
4.39 *Applied voltage 30 V in a complete reactor with turbulent flow on the upper horizontal side of the first bipolar electrode:* ***a)*** *Local current density of the reactions producing* Cl_2, O_2 *and* H_2 *also the normal vector of electrolyte current density is plotted. and* ***b)****Overpotential of the aforementioned reactions.* . . . 64

4.40 *Applied voltage 30 V in a complete reactor with turbulent flow, local current density of the reactions producing* Cl_2, O_2 *and* H_2 *also the normal vector of electrolyte current density is plotted on* ***a)*** *the upper horizontal side of the third bipolar electrode and* ***b)*** *the lower horizontal side of the third bipolar electrode.* 65
4.41 *Chlorine* (Cl_2) *concentration distribution at the outlet of the full reactor.* 66
4.42 *Applied potential 30 V and OER with 1.5 apparent transfer coefficient in a complete reactor with turbulent flow on the upper horizontal side of the third bipolar electrode:* ***a)*** *Local current density of the reactions producing* Cl_2, O_2 *and* H_2 *(also the normal vector of electrolyte current density is plotted) and* ***b)*** *Overpotential of the aforementioned reactions.* . . 66

List of Tables

3.1 *Boundary conditions in case of laminar flow using Navier-Stokes equation.* . . . 26
3.2 *Boundary conditions in case of Secondary Current Distribution model.* . . . 29
3.3 *Boundary conditions in case of Multi-ion Transport in Dilute Electrolyte Solutions.* . . . 29

4.1 *Inlet concentrations and diffusion coefficients for Cl^-, Na^+, H^+, OH^-, Cl_2, HOCl and OCl^-.* . . . 33
4.2 *Kinetic parameters for electrode reactions of Cl_2, $O_2$and H_2 production.* . . . 34
4.3 *Mesh properties for the examined cases.* . . . 35
4.4 *Mesh properties for the examined case.* . . . 42
4.5 *Mesh properties for the complete reactor.* . . . 62

Chapter 1

Introduction

1.1 Generalities

Along with domestic and international freight, ships carry ballast water as well. This is necessary to ensure ship's stability and balance as well as maintain stress loads within acceptable limits. Ships without cargo fill their tanks with ballast water, whereas in the presence of cargo ballast water is discharged.

Ballast water may be saltwater, freshwater or brackish water which may carry sediments and a wide variety of organisms. The sediments taken aboard along with ballast water contain organisms even when ballast water is exchanged at sea. Most of these organisms, including bacteria, phytoplankton, zoo-plankton, macro-algae, plants, fishes e.t.c., do not survive the journey or the new environmental conditions where they are discharged. However, some species survive in the host environment under favorable circumstances. Once established, organisms permanently alter ecosystems. At this point, the environmental influence of these species often results in unpredictable ecological, economic and social impacts.

Globally, the transfer of ballast water is estimated to be 10 billion metric tons annually. The International Marine Organization (IMO), which regulates the international shipping industry, adopted guidelines for ballast water management in 1997, in an attempt to prevent the introduction of harmful aquatic organisms and pathogens by requiring ballast water exchange (IMO 1997). Later, The International Convention for the Control and Management of Ships Ballast Water & Sediments (BWM Convention) was also adopted in 2004. As a result, 30 countries, representing 35% of the world's shipping tonnage, must ratify the convention[1].

---

[1] Lacasa et al. 2013

In response to the above, a number of technologies have been developed and commercialized by different vendors (e.g. ERMA FIRST ESK Engineering Solutions S.A). Many have their basis in land-based applications for municipal, industrial water and of fluent treatment and have been adapted to meet the requirements of the BWM Convention and shipboard operation. The methodology recommended by the IMO guidelines for ballast water treatment involves its exchange to reduce the risk of transfer of harmful aquatic organisms. Nevertheless, this method has ship-safety limitations because it is not completely effective in removing organisms from ballast water. Thus, effective ballast water management and/or treatment methods should be developed in order to replace the ballast water exchange at sea. So far, several technologies have been suggested for ballast water treatment, including filtration, irradiation with ultraviolet light , sterilization with ozone, addition of biocides to ballast water to kill organisms, sonication and disinfection with chlorine species (or hydrogen peroxide). In this thesis, focus will be laid to disinfection with chlorine which is electrochemically produced by electrolysis.

The electrochemical production of chlorine, by electrolysis of brine, is one of the major processes in the chemical industry and one of the earliest commercial exploitations of an electrochemical reaction on a large scale. Electrochemical disinfection can be defined as the eradication of microorganisms using an electric current passed through the water by means of suitable electrodes. The advantages of electrochemical water disinfection in comparison to other chemical methods include:

i simplicity of the equipment,

ii easy automation of the process,

iii the fact that additional chemicals are not required since the disinfectant dose can be easily controlled varying the current density applied and

iv the relatively low current requirement that may allow the use of green energy sources such as solar cells or fuel cells.

In the case of saline water treatment, electrochemical disinfection takes advantage of the electrolytic production of chlorine species such as hypochlorite and hypochlorous acid (i.e., electrochlorination)

A typical reactor, in small-scale, implementing electrolysis for chlorine production can be seen in Figure 1.1. The reactor contains a configuration of feeder and bipolar electrodes. Feeder electrodes are located on the two edges of the reactor, a pair of feeder electrodes on the left and a triplet

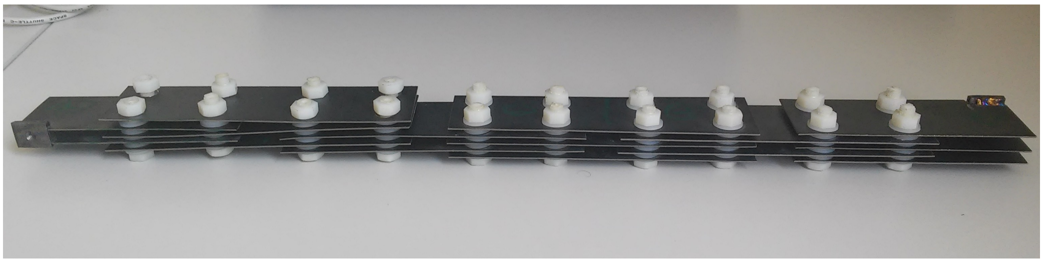

Figure 1.1: *Small-scale electrochemical reactor implementing electrolysis for chlorine production.*

feeder electrodes on the right, as it can be seen in Figure 1.1. Also, feeder electrodes, on each edge, can be either anodes or cathodes with known potential depending on the applied voltage (considering a grounded cathode). The remaining electrodes are bipolar. The reactor in Figure 1.1 contains two consecutive groups of five bipolar electrodes. The bipolar electrode, as the name denotes, acts as both an anode and cathode. Therefore, during operation, bipolar electrodes are reversibly polarized as can be seen in Figure 1.2.

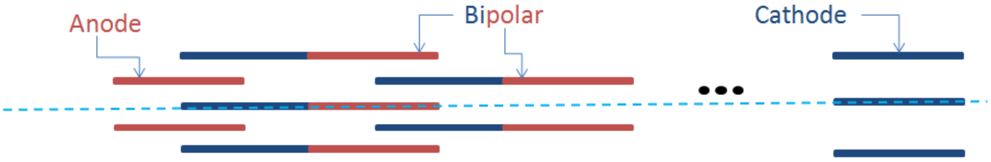

Figure 1.2: *Polarization of bipolar electrodes during reactor operation.*

The aim of the present study is the modeling of the above electrochemical reactor used for the production of chlorine, by implementing the COMSOL Multiphysics software.

1.2 Electrode Materials

Historically, carbon and magnetite anodes were the materials initially used for production of chlorine but their lifetimes and anode overvoltage characteristics are less than favorable; considerable consumption of the C anode material occurs through oxidation to CO and CO_2, and erosion. However, since 1900, graphite has been extensively used prior to the advent of metal anodes in the late 1960s. Modern metal anode technology started with the development of Pt-coated Tungsten anodes by Stevens in 1913.

Nevertheless, a technological breakthrough in the history of electrolytic chlorine production is the presence of Dimensional Stable Anodes (DSA), which were invented by H.B. Beer in 1965 and were then developed and industrialized by De Nora as a result of their investigation on metallic oxide coatings, as anode catalysts, for chlorine and oxygen evolution reactions.

The commercially available DSA consists of RuO_2 as active component, inert oxide (e.g. TiO_2) as stabilizer and coated (with a relatively thick layer) onto titanium substrate (inert support). Generally, each component plays a well defined role: electrocatalyst, stability promoter, selectivity enhancer, etc. The action of each component depends on its crystalline and electronic structure, and on the degree of intermixing with the other components. The benefit of using a conductive titanium substrate is that a fixed inter-electrode gap can be maintained during the long-term operation of the electrolytic cell. Moreover, titanium is adequately durable to general acidic corrosion. Furthermore, RuO_2 exhibits excellent corrosion resistance and low overpotential for anodic chlorine evolution reaction. In order to prepare this kind of electrode coatings, a thermal decomposition method of suitable precursors, is generally used.

It is well understood that the selection of a proper anodic material is a key point in a electrolytic process. More specifically, the nature of the electrode material affects both Cl_2 yield and purity, since the chlorine evolution reaction, ClER, is influenced by the presence of O_2 from the oxygen evolution reaction, OER. To achieve high Cl_2 current efficiency, it is necessary to work at low pH values of the electrolyte and with electrode materials that show, in principle, significant overpotentials for the OER. Thus, electrode selectivity for the ClER remains a problem of technological interest, although a broad fundamental and applied research of ClER is available.

Overall, DSA-type electrodes have been well succeeded for almost 40 years, mainly due to their versatile electrocatalytic properties and stability. These electrodes have shown significant activity for all common gas evolution reactions (O_2 and Cl_2), long life, good Cl_2 overvoltage-current-density characteristics and present good efficiencies in the production of hypochlorite, which is critical for several uses of electrochemical technologies in many environmental applications.

1.3 Chlorine Evolution Reaction

From the point of view of fundamental electrochemistry, the anodic Cl_2 evolution reaction has many interesting features:

(a) stoichiometrically speaking, it is one of the simplest gas evolution reactions similar to H_2 cathodic production, requiring the discharge of two Cl^- ions leading to the formation of a diatomic molecule after a chemical or electrochemical "recombination" type of reaction,

(b) it proceeds with Coulombic yields near 96% except in dilute Cl^- solutions where some O_2 and chlorine oxides may be evolved,

(c) it is an anodic reaction with otherwise similar mechanistic features to those of the cathodic H_2 evolution reaction for which much fundamental kinetic and electro catalytic information exists,

(d) like the H_2 evolution reaction, its kinetics are sensitive to the electrocatalytic and adsorptive properties of the anode electrode material, both for the reactant ion Cl^- and the intermediate $Cl^\bullet$ and

(e) because it is an anode reaction, it normally proceeds in aqueous solution at electrode surfaces that are, in some way, covered or partially covered with an electrolytically generated oxide film or, in certain cases, a specially formed (e.g., thermally) oxide film as with proprietary DSA electrodes.

Generally, the thermodynamics of the chlorine-chloride reaction at equilibrium:

$$\mathrm{Cl}_2 + 2e \rightleftharpoons 2\mathrm{Cl}^- \tag{1.1}$$

are well established. The recommended standard reversible potential is 1.35828 V versus E_H (Stockholm convention), corresponding to a Nernst equation

$$E_{\mathrm{Cl}_2} = E^{\circ}_{\mathrm{Cl}_2} - \frac{RT}{F} \ln \left[\frac{\alpha_{\mathrm{Cl}^-}}{f^{1/2}_{\mathrm{Cl}_2}} \right] \tag{1.2}$$

where α_{Cl^-} is the activity of Cl^- ions and $f^{1/2}_{\mathrm{Cl}_2}$ the fugacity of Cl_2 gas.

Reaction 1.1 is relatively reversible and can be established as a practical reversible electrode at platinized Pt electrodes or platinized-iridized surfaces in a way similar to that employed for H_2-H^+ reversible electrodes. Reaction 1.1 has exchange current densities at catalytic noble metals of 10^{-3}-10^{-4} A/cm^2 (10^1-10^0 A/m^2)[1].

---

[1] Payer and Neumann 1976

In comparison with the knowledge of the kinetics and pathways of the mechanistically analogous H_2 evolution reaction, less is known about for the anodic Cl_2 evolution reaction. Similarly, much less is known about the role of adsorption of the reactant Cl^- ion and the discharged intermediate $Cl^\bullet$ in the mechanism of this reaction at various electrodes.

The recent development of the so-called dimensionally stable anodes, presently used in the chloralkali industry, has spurred considerable activity in understanding the kinetics of chlorine evolution and in developing other "nonmetallic surfaces" for various kinds of electrode reactions.

At the potentials at which Cl_2 is normally evolved (> 1.36 V), most metal anodes are covered or partially covered with a surface oxide film, Figure 1.3 (Bockris, Conway, and White 1982). In all commercially used electrodes, the surface oxide is fully formed as a film of substantial thickness. The anodic Cl_2 evolution process will therefore take place on such a surface whose adsorptive and catalytic properties will be substantially different from those of the corresponding free metal electrode surfaces.

In addition to the formation of surface oxide films with adsorbed Cl^- ion, an anodic corrosion partial process of metal or metal oxide dissolution may sometimes take place giving rise to a continuously changing state of the metal surface. Thus with metallic Pt or Ru surfaces, appreciable dissolution of the metals as complex chlorides can occur at high current densities in strong Cl^- solutions.

In anodic Cl_2 evolution, the reactant ion, Cl^- is not simply the initial reactant in the overall process but it also modifies the state of the anode surface on which it is discharged. On any bare metal sites, Cl^- is normally strongly chemisorbed. This leads to strong inhibition of the formation of monolayer surface oxides, especially at Pt or Rh, that would normally be complete at potentials less than those required for Cl_2 evolution. So, depending on the concentration of Cl^- and the potential, e.g., at Pt, the extent of surface oxide film formation in the presence of Cl^- can be much less than a monolayer. Therefore, Cl^- adsorption changes the properties of the electrode surface on which the reaction of conversion of Cl^- to chlorine occurs.

In addition, Cl^- adsorption will tend to increase with increasing positive potentials of the electrode and thus maintain competitive adsorption with respect to electrodeposition of monolayer or multilayer surface oxide, into the potential range where appreciable rates of Cl_2 evolutions arise. The normal increase of extent of surface oxidation with positive potential is thus diminished.

Finally, at high current densities in commercial Cl_2 evolution at 95°C from brine, the current efficiency is usually better than 98%, even though there are possibilities for the anodic generation of ClO and ClO_2 gases in

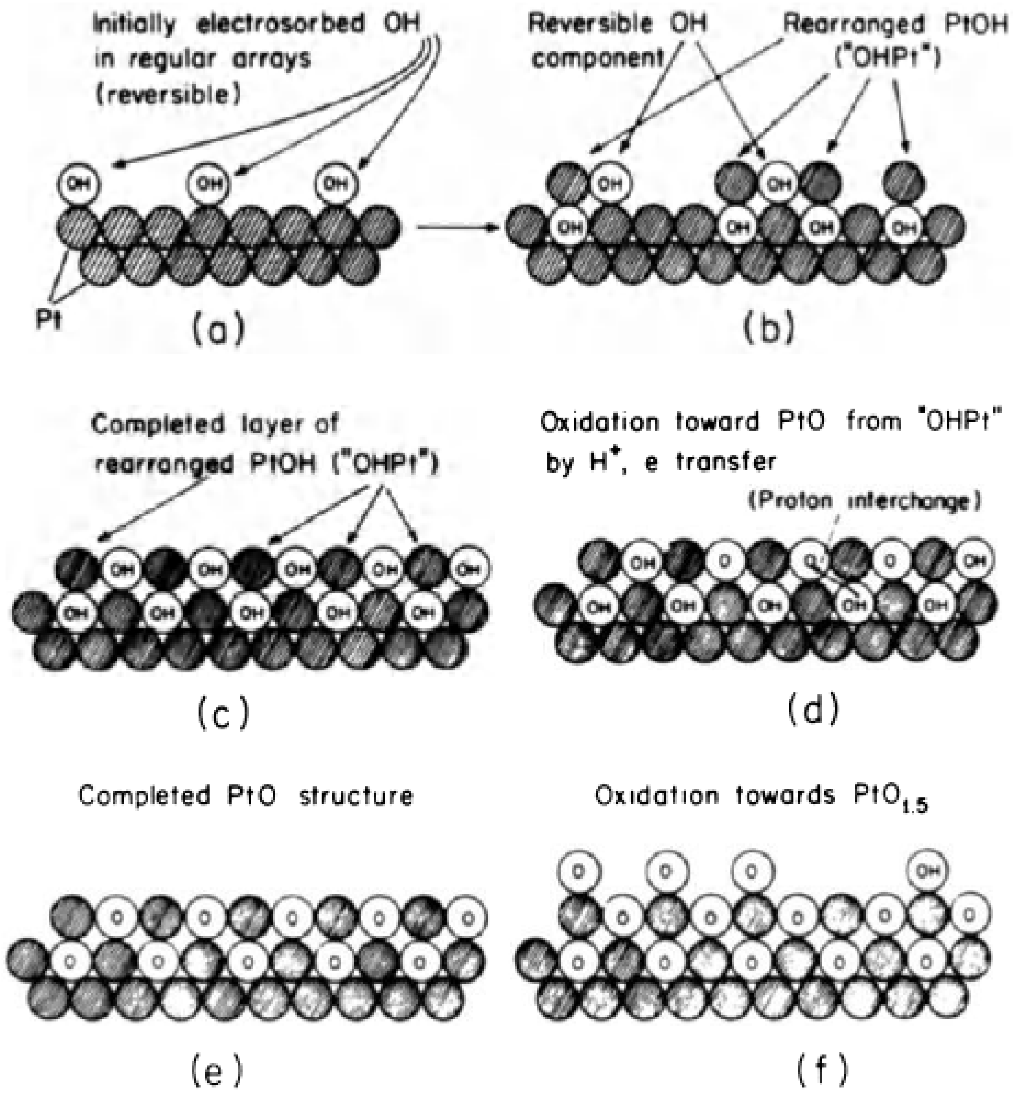
Initially electrosorbed OH in regular arrays (reversible)
Pt
OH
(a)
Reversible OH component
Rearranged PtOH ("OHPt")
(b)
Completed layer of rearranged PtOH ("OHPt")
(c)
Oxidation toward PtO from "OHPt" by H⁺, e transfer
(Proton interchange)
O
(d)
Completed PtO structure
(e)
Oxidation towards PtO1.5
(f)

Figure 1.3: *Model for surface oxidation of Pt: transition from OH monolayer, through rearranged OH/Pt state, to O/Pt-PtO structure.*

addition to Cl_2 and O_2, giving rise to hazardous conditions.

1.4 Oxygen Evolution Reaction

The overall four-electron reductions of O_2 in acid and alkaline aqueous solutions are, respectively,

$$\begin{aligned} O_2 + 4H^+ + 4e^- &\rightleftharpoons 2H_2O \quad (E^\circ_{\mathrm{NHE}})_{298} = 1.229\mathrm{V} \\ O_2 + 2H_2O + 4e^- &\rightleftharpoons 4OH^- \quad (E^\circ_{\mathrm{NHE}})_{298} = 0.401\mathrm{V} \end{aligned} \tag{1.3}$$

where the standard reduction potentials have been calculated relative to the standard hydrogen electrode (SHE, NHE, or RHE) from the standard free energy of formation of water and OH^- ions. Moreover, the Nernst equation in acidic solution for O_2 evolution is:

$$E_{O_2} = E^\circ_{O_2} + \frac{RT}{4F} \ln \left[\alpha^4_{H^+} \cdot f_{O_2} \right] \tag{1.4}$$

where α_{H^+} is the activity of H^+ ions and f_{O_2} the fugacity of O_2 gas.

Thermodynamically, in aqueous solution, O_2 (standard reversible potential 1.229 V) should be evolved before Cl_2. However, the exchange current densities for Cl_2 evolution on noble metals and carbon are usually substantially greater than those of O_2 evolution, so Cl_2 is normally the preferred anodic product in the electrolysis of aqueous Cl^- solutions. Since oxygen evolution, and in most instances also O_2 electroreduction, occur on electrode surfaces covered with an adsorbed oxygen species or an oxide layer, the properties of such layers control the mechanisms and electrocatalytic activity of the electrode for these processes.

Moreover, as discussed previously, Cl^- adsorption has a major effect on the development of the surface oxide film which is anodically formed at noble metals and changes the critical state of this film which is usually required for the onset of significant rates of O_2 evolution. Thus Cl_2 evolution normally becomes even more favored over O_2 evolution since there is a coupling between the Cl_2 reaction, through Cl^- ion adsorption effects on the oxide film, and the oxygen evolution reaction on the same surface. Therefore, coulombic efficiency cannot be calculated simply from the sum of Cl_2 and O_2 currents based on independently determined Tafel parameters for these reactions. Additionally, O_2 can also be formed by parallel reactions (anodic oxidation of OCl^- to ClO_3) from Cl^- solutions.

The studies on the mechanism of the reaction of oxygen evolution on most simple oxide electrodes like RuO, have shown that the Tafel slope is commonly around 40 mVs^{-1}, which indicates that the rate determining step is the transfer of the second electron. [1]

In dilute solutions, Cl_2 evolution is less favored; firstly, because its exchange current is diminished for low Cl_2 concentrations, determined by the transfer coefficient of the reaction and secondly, because at sufficiently high current densities, the reaction will become diffusion-controlled, O_2 evolution from water discharge will eventually become the predominant reaction and the current efficiency for Cl_2 evolution will be $\ll$100%. A further factor favoring Cl_2 over O_2 evolution is the lower Tafel slope for the former reaction thus giving preferential evolution of Cl_2 over O_2 at high potentials.

If low Cl^- concentrations are to be used, e.g., in reaction-order measurements over a wide range of concentrations, then experiments should be conducted at a rotating-disk electrode where diffusion problems can be minimized, if not eliminated. If the diffusion-limited current for Cl^- oxidation is exceeded, coevolution of O_2 will, occur at higher potentials with a diminution of current efficiency for Cl_2 formation.

1.5 Bipolar Electrodes

Bipolar electrode behavior of conducting bodies is a phenomenon widely exploited in industrial applications. Examples can be found in such fields as organic electrosynthesis, elaboration of micro-conductive paths, supported catalyst metal particle technology but also electrolysis for chlorine production.

Beyond a critical extent of polarization of such an electrode, i.e. in a sufficiently strong lateral electric field, the overpotentials become sufficiently high to induce noticeable electrolysis: the spatial variation of the electrode / solution potential provokes oxidation on one side of the electrodes, coupled with reduction at the other. More specifically, high overpotential values, either positive or negative give rise to strong bipolar, either anodic (production of chlorine and oxygen) or cathodic (production of hydrogen), currents. On the other hand, low difference between bipolar electrode and solution potentials along its surface (on the axis of the lateral electrical field), leads to low overpotentials which give rise to low currents on the bipolar electrode.

Therefore, for sufficiently strong fields, the bipolar electrodes inside the reactor produce chlorine and oxygen anodically at the electrode side facing the low electric field and hydrogen cathodically at the electrode side facing the high electric field, thus giving rise to a flow of electrons through the bipolar electrode body. The effective bipolar faradaic current is derived from the spatial integral of either the local cathodic or the local anodic current density, the anodic and cathodic current integrals being necessarily identical.

---

[1] Jin and Ye 1996

Chapter 2

Reactions Kinetics

2.1 Kinetics of Chlorine Evolution Reaction

In comparison with the extent of published work on the Hydrogen (H_2) Evolution Reaction since 1904 by Tafel, relatively little work exists on the mechanisms of the Chlorine (Cl_2) Evolution Reaction. Also, the interpretation of experimental kinetic data is more complex than that for the H_2 evolution reaction because of the following:

- the presence of oxide films,
- their changing catalytic properties with potential and time,
- adsorption of Cl^- and their possible incorporation in growing oxide films and
- some dissolution of the oxide film and/or substrate metal.

Nevertheless, the steps in anodic chlorine (Cl_2) evolution are analogous to those in cathodic hydrogen (H_2) evolution, except that the ion discharge step(s) are anodic rather than cathodic. The following are obvious steps and mechanisms, at metal surface or surface oxide sites M, that have been considered by various workers[1],

$$\mathrm{Cl}^- + \mathrm{M} \underset{k_{-1}}{\overset{k_1}{\rightleftharpoons}} \mathrm{M}\cdot\mathrm{Cl}^\bullet_{\mathrm{ads}} + e^- \quad \text{Volmer} \tag{2.1}$$

$$2\mathrm{M}\cdot\mathrm{Cl}^\bullet{}_{\mathrm{ads}} \overset{k_2}{\rightarrow} 2\mathrm{M} + \mathrm{Cl}_2\uparrow \quad \text{Tafel} \tag{2.2}$$

---

[1] Bockris, Conway, and White 1982

or

$$\mathrm{M} \cdot \mathrm{Cl}^{\bullet}{}_{\mathrm{ads}} + \mathrm{Cl}^{-} \rightarrow \mathrm{M} + \mathrm{Cl}_2 \uparrow + e^{-} \quad \text{Heyrovsky} \tag{2.3}$$

The first two steps (2.1 and 2.2) consist the Volmer-Tafel mechanism. On the other hand, the pathway consisting of steps 2.1 and 2.3 is the Volmer-Heyrovsky mechanism. It is worth mentioning that step 2.3 can proceed faster than 2.2.

A third type of mechanism was considered by Krishtalik, based on the possibility of formation of the chloronium ion Cl^{+}.

$$\mathrm{Cl}^{-} + \mathrm{M} \rightarrow \mathrm{M} \cdot \mathrm{Cl}^{\bullet}{}_{\mathrm{ads}} \tag{2.4}$$

$$\mathrm{M} \cdot \mathrm{Cl}^{\bullet}{}_{\mathrm{ads}} \rightarrow \mathrm{M} \cdot \mathrm{Cl}^{+}{}_{\mathrm{ads}} + e^{-} \quad \text{or} \quad \mathrm{M} + \mathrm{Cl}^{+} + e^{-} \tag{2.5}$$

$$\mathrm{M} \cdot \mathrm{Cl}^{+}{}_{\mathrm{ads}} \quad \text{or} \quad \mathrm{Cl}^{+} + \mathrm{Cl}^{-} \rightarrow \mathrm{Cl}_2 \uparrow \tag{2.6}$$

For each mechanism, if the rate determining step is known, a Butler-Volmer equation can be derived. Bockris 1955 describes the development of a Butler–Volmer equation for a multi-step reaction. Taking into consideration the Volmer-Tafel mechanism and assuming that the *rds* is the chemical step (Tafel step 2.2) a description of the derived Butler-Volmer equation is the following.

In a multi-step electron-transfer reaction, the step with the lowest servicing rate produces the largest queue and, indeed, the total queue is virtually a simple multiple of the queue at the *rds*. So, in the steady state, all n steps proceed at the rate of the rate-determining step i_r and the total net current is:

$$i = n i_r = n(\overrightarrow{i_r} - \overleftarrow{i_r}) \tag{2.7}$$

where n is the number of single-electron transfer steps in the overall reaction. In the Volmer-Tafel mechanism the first step is electrochemical, which consists of two single electron transfer steps and the second step is chemical (not electron exchange). So, in the overall reaction $n = 2$.

In order to develop the Butler–Volmer equation for a multi-step reaction, expressions for $\overrightarrow{i_r}$ and $\overleftarrow{i_r}$ must be found. Thus, the total net current is:

$$i = i_r = \overrightarrow{i_r} - \overleftarrow{i_r} = F k_2 [M \cdot \mathrm{Cl}^{\bullet}{}_{\mathrm{ads}}]^2 - F k_{-2} C_{\mathrm{Cl}_2} \tag{2.8}$$

Since, the Volmer step (step 2.1) precedes the *rds* step, it can be considered in steady state:

$$i_V = \overrightarrow{i_V} - \overleftarrow{i_V} = 2Fk_1 C^2_{\mathrm{Cl}^-} e^{2(1-a_a)\frac{F}{RT}E} - 2Fk_{-1}[\mathrm{M}\cdot\mathrm{Cl}^{\bullet}{}_{\mathrm{ads}}]^2 e^{-2a_c\frac{F}{RT}E} = 0 \tag{2.9}$$

hence $[\mathrm{M}\cdot\mathrm{Cl}^{\bullet}_{\mathrm{ads}}]$ can be calculated:

$$[\mathrm{M}\cdot\mathrm{Cl}^{\bullet}_{\mathrm{ads}}]^2 = \frac{k_1}{k_{-1}} C^2_{\mathrm{Cl}^-} e^{2\frac{F}{RT}E} \tag{2.10}$$

Thus, $[\mathrm{M}\cdot\mathrm{Cl}^{\bullet}_{\mathrm{ads}}]$ can be substituted to the total net current (Equation 2.8):

$$i = Fk_2\frac{k_1}{k_{-1}} C_{\mathrm{Cl}^-}{}^2 e^{2\frac{F}{RT}E} - Fk_{-2}C_{\mathrm{Cl}_2} \tag{2.11}$$

Equation 2.11 can be further manipulated, in order to derive a Butler-Volmer equation. Assuming that the cell potential is equal to the equilibrium potential ($E = E_{\mathrm{eq}}$), the total net current becomes zero ($i = 0$) and concentrations take the equilibrium concentration values ($c = c^*$).

$$\text{if} \quad E = E_{\mathrm{eq}} \qquad \text{then} \quad i = i_{0_a} - i_{0_c} = 0 \ (\textit{Equation } 2.11)$$

So, $i = i_{0_a} = i_{0_c}$ and i_{0_c} can be defined as:

$$\begin{aligned} i_{0_a} &= Fk_2\frac{k_1}{k_{-1}}(C^*_{\mathrm{Cl}^-})^2 e^{2\frac{F}{RT}E} \\ i_{0_c} &= Fk_{-2}C^*_{\mathrm{Cl}_2} \end{aligned} \tag{2.12}$$

Hence, the exchange current density i_0 can be calculated:

$$i_0 = i_{0_a} = i_{0_c} \tag{2.13}$$

Now, Equation 2.11 can take the known form of Butler-Volmer:

$$i = i_0\Big(\Big(\frac{C_{\mathrm{Cl}^-}}{C^*_{\mathrm{Cl}^-}}\Big)^2 e^{2\frac{F}{RT}(E-E_{\mathrm{eq}})} - \frac{C_{\mathrm{Cl}_2}}{C^*_{\mathrm{Cl}_2}}\Big) \tag{2.14}$$

Equation 2.11 can be even further manipulated. Assuming that the cell potential is equal to the standard potential ($E = E^{\circ}$), the total net current becomes zero ($i = 0$) and concentrations are equal to unity. Thus, an alternative form of the total net current is:

$$i = Fk_2 \frac{k_1}{k_{-1}} e^{2\frac{F}{RT}E^\circ} (C_{\mathrm{Cl}^-})^2 e^{2\frac{F}{RT}(E-E^\circ)} - Fk_{-2}C_{\mathrm{Cl}_2} \tag{2.15}$$

also, an extra equation, relating the reaction constants, is arising:

$$k_2 \frac{k_1}{k_{-1}} e^{2\frac{F}{RT}E^\circ} = k_{-2} \tag{2.16}$$

2.2 Kinetics of Oxygen Evolution Reaction

The oxygen electrode has been the subject of extensive investigations over the past century. The irreversibility of the cathodic and anodic reactions in aqueous solutions has imposed severe limitations on the information which can be obtained concerning the pathways from electrochemical kinetic studies. In most instances at current densities practical for kinetic studies, the current-voltage data are not sensitive to the back-reaction and hence yield information only up to the rate-controlling step, which usually occurs early in the multiple-step reaction sequence. Further the reduction and oxidation processes are usually studied only at widely separated potentials and thus the surface conditions differ sufficiently such that the reduction and oxidation pathways are probably not complementary. The situation is made all the more complicated by the large number of possible pathways for the oxygen electrode reactions (Conway et al. 1983).

Treatment of consecutive electrochemical reactions differs from that of ordinary consecutive reactions in two ways. Firstly, if it is assumed that the current density and time used are such that no pH change occurs in the vicinity of the electrode, the concentration of reactants in the initial state of the reaction (e.g. OH^- ions) remains constant throughout the reaction. Secondly, the rate constants of reactions involving charged components depend on potential. Thus k_i, the electrochemical rate constant of the forward step of the ith (anodic) reaction in a series, is equal to

$$k_i e^{a_a EF/RT} \tag{2.17}$$

where k_i is the rate constant for this electrochemical step when the Galvani metal-solution PD is zero, the step involves the transfer of n electrons, a_a

is the symmetry factor and $\Delta\phi$ the Galvani potential between the electrode and the charge center of the first layer of ions.

Bockris 1955 gives five paths for the electrolytic evolution of oxygen at anodes and yields limiting expressions for the dependence of the current density (or rate) of the reaction upon electrode potential which are diagnostic of the various rate controlling steps assumed.

The Oxide Path

$$\mathrm{OH^- + M \underset{\nu_{-1}}{\overset{\nu_1}{\rightleftharpoons}} MOH} + e^- \tag{2.18}$$

$$\mathrm{2MOH \underset{\nu_{-2}}{\overset{\nu_2}{\rightleftharpoons}} MO + M + H_2O} \tag{2.19}$$

$$\mathrm{2MO \underset{\nu_{-3}}{\overset{\nu_3}{\rightleftharpoons}} 2M + O_2} \tag{2.20}$$

The Electrochemical Oxide Path

$$\mathrm{OH^- + M \underset{\nu_{-1}}{\overset{\nu_1}{\rightleftharpoons}} MOH} + e^- \tag{2.21}$$

$$\mathrm{MOH + OH^- \underset{\nu_{-2}}{\overset{\nu_2}{\rightleftharpoons}} MO + H_2O} + e^- \tag{2.22}$$

$$\mathrm{2MO \underset{\nu_{-3}}{\overset{\nu_3}{\rightleftharpoons}} 2M + O_2} \tag{2.23}$$

The Hydrogen Peroxide Path

$$\mathrm{OH^- + M \underset{\nu_{-1}}{\overset{\nu_1}{\rightleftharpoons}} MOH} + e^- \tag{2.24}$$

$$\mathrm{2MOH \underset{\nu_{-2}}{\overset{\nu_2}{\rightleftharpoons}} MH_2O_2 + M} \tag{2.25}$$

$$\mathrm{MOH + MH_2O_2 \underset{\nu_{-3}}{\overset{\nu_3}{\rightleftharpoons}} MHO_2 + H_2O} \tag{2.26}$$

The Electrochemical Metal Peroxide Step

$$\mathrm{OH^- + M \underset{\nu_{-1}}{\overset{\nu_1}{\rightleftharpoons}} MOH} + e^- \tag{2.27}$$

$$\mathrm{2MOH \underset{\nu_{-2}}{\overset{\nu_2}{\rightleftharpoons}} MO + H_2O} \tag{2.28}$$

$$\mathrm{MO + OH^- \underset{\nu_{-3}}{\overset{\nu_3}{\rightleftharpoons}} MHO_2} \tag{2.29}$$

$$\mathrm{2MHO_2 + MOH \underset{\nu_{-4}}{\overset{\nu_4}{\rightleftharpoons}} MO + O_2 + H_2O + M} \tag{2.30}$$

The Metal Peroxide Path

$$\mathrm{OH^- + M \underset{\nu_{-1}}{\overset{\nu_1}{\rightleftharpoons}} MOH} + e^- \tag{2.31}$$

$$\mathrm{2MOH \underset{\nu_{-2}}{\overset{\nu_2}{\rightleftharpoons}} MO + H_2O} \tag{2.32}$$

$$\mathrm{MO + MOH \underset{\nu_{-3}}{\overset{\nu_3}{\rightleftharpoons}} MHO_2} \tag{2.33}$$

$$\mathrm{MHO_2 + MOH \underset{\nu_{-4}}{\overset{\nu_4}{\rightleftharpoons}} O_2 + H_2O + 2M} \tag{2.34}$$

One can obtain the overall forward rate of each path, for a predetermined *rds*, using the method that Bockris provides. Taking into consideration the Electrochemical Oxide Path with step 2.19 as the rate determining, the development of the overall forward rate is following. Assuming an acidic aqueous solution, the Electrochemical Oxide Path can be written as:

$$\begin{aligned}
&a)\quad \mathrm{M + H_2O \underset{k-1}{\overset{k_1}{\rightleftharpoons}} MOH + H^+}e^- \\
&b)\quad \mathrm{MOH \underset{k_{-2}}{\overset{k_2}{\rightleftharpoons}} MO + H^+} + e^- \quad \text{[RDS]} \\
&c)\quad \mathrm{2MO \underset{k_{-3}}{\overset{k_3}{\rightleftharpoons}} 2M + O_2}
\end{aligned} \tag{2.35}$$

obtaining the forward and backward rates of each step,

$$\begin{aligned}
v_1 &= k_1(1 - x_{\mathrm{MOH}})e^{a_a f E} \\
v_{-1} &= k_{-1}C_{\mathrm{MOH}}C_{\mathrm{H^+}}e^{a_c f E} \\
v_2 &= k_2 C_{\mathrm{MOH}}e^{a_a f E} \\
v_{-2} &= k_{-2}C_{\mathrm{MO}}C_{\mathrm{H^+}}e^{a_c f E} \\
v_3 &= k_3 {C_{\mathrm{MOH}}}^2 \\
v_{-3} &= k_{-3}
\end{aligned} \tag{2.36}$$

where $x_{\mathrm{MOH}} = k^1 C_{\mathrm{MOH}}$ is the fraction of the surface covered with MOH.

To obtain an expression for the forward rate of a generic consecutive multi-step reaction, one writes

$$v = w_1 - w_{-1}C_{x(1)} \tag{2.37}$$

where $w_1 = k_1 C_1$ and C_1 is the concentration of the stable, known entity in the initial state and $C_{x(1)}$ is the concentration of the radical produced in the first stage of the reaction. Similarly,

$$v = w_2 C_{x(1)} - w_{-2}C_{x(2)} \tag{2.38}$$

where $x(2)$ is the species produced by the forward direction of the second step. Analogously,

$$v = w_n C_{x(n-1)} - w_{-n} C_{x(n)} \tag{2.39}$$

where $x(n-1)$ and $x(n)$ are the species produced by the forward direction of the n-1 and n step. The above can be more understood in Appendix A.

Once the entities w_i have been introduced, the forward and backward reaction rates v_i of Equation 2.36 can now be converted as:

$$\begin{aligned} w_1 &= k_1 e^{a_a f E} \\ w_2 &= k_2 e^{a_a f E} \\ w_{-2} &= k_{-2} C_{\mathrm{H}^+} e^{a_c f E} \\ w_3 &= k_3 C_{\mathrm{MOH}} \\ w_{-3} &= k_{-3} \end{aligned} \tag{2.40}$$

The calculation of the entity w_{-1} is tricky, for this reason will be presented separately. The overall rate is equal to the rate of the first step which can be obtained by subtraction of the backward from the forward rate of the first step:

$$\begin{aligned} v =& v_1 - v_{-1} = k_1(1 - x_{\mathrm{MOH}}) e^{a_a f E} - k_{-1} C_{\mathrm{MOH}} C_{\mathrm{H}^+} e^{a_c f E} = \\ =& [k_1 e^{a_a f E}] - [k_1 x_{\mathrm{MOH}} e^{a_a f E} + k_{-1} C_{\mathrm{MOH}} C_{\mathrm{H}^+} e^{a_c f E}] = \\ =& [k_1 e^{a_a f E}] - [k_1 k^1 C_{\mathrm{MOH}} e^{a_a f E} + k_{-1} C_{\mathrm{MOH}} C_{\mathrm{H}^+} e^{a_c f E}] \end{aligned} \tag{2.41}$$

Thus, the entity w_{-1} becomes:

$$w_{-1} = k_1 k^1 e^{a_a f E} + k_{-1} C_{\mathrm{H}^+} e^{a_c f E} \tag{2.42}$$

According to Christiansen 1936 equations similar in form to 2.37, 2.38 and 2.39 can be written for each of the consecutive reactions and for n simultaneous equations involving v and (n-1) X's. The solution, of the forward rate of the overall reaction, to such a series of equations is given by:

$$\frac{1}{v} = \frac{1}{w_1} + \frac{w_{-1}}{w_1 w_2} + \frac{w_{-1} w_{-2}}{w_1 w_2 w_3} + \ldots + \frac{w_{-1} w_{-2} \ldots w_{n-1}}{w_1 w_2 w_3 \ldots w_n} \tag{2.43}$$

The above Equation 2.43 can also be more well understood in Appendix A.

Finally, for the Electrochemical Oxide Path, with step 2.19 as the rate determining, assuming that k_2, $k_{-2} \to 0$ and $k_1 c_{\mathrm{H}^+} e^{a_c f E} \gg k_1 k^1 e^{a_a f E}$ the forward rate of the overall reaction (consisting by three steps) is:

$$v = \frac{k_1 k_2}{k_1} \frac{1}{C_{\mathrm{H}^+}} e^{1.5 \frac{F}{RT} E} \tag{2.44}$$

Hence, the overall current for the forward reaction is:

$$i = 2F\frac{k_1 k_2}{k_1}\frac{1}{C_{\mathrm{H}^+}}e^{1.5\frac{F}{RT}E} \tag{2.45}$$

which can take the familiar form,

$$i = i_0\frac{C^*_{\mathrm{H}^+}}{C_{\mathrm{H}^+}}e^{1.5\frac{F}{RT}(E-E_{\mathrm{eq}})} \tag{2.46}$$

where i_0 is the exchange current density:

$$i_0 = 2F\frac{k_1 k_2}{k_1}\frac{1}{C^*_{\mathrm{H}^+}}e^{1.5\frac{F}{RT}E_{\mathrm{eq}}} \tag{2.47}$$

Similar to the above analysis for the development of the overall current for the forward reaction of the Electrochemical Oxide Path, the overall current for the Oxide Path, assuming the first step 2.18 as rate determining, is,

$$i = Fk_1 e^{0.5\frac{F}{RT}E} \tag{2.48}$$

which can take the familiar form,

$$i = i_0 e^{0.5\frac{F}{RT}(E-E_{\mathrm{eq}})} \tag{2.49}$$

where i_0 is the exchange current density:

$$i_0 = Fk_1 e^{0.5\frac{F}{RT}E_{\mathrm{eq}}} \tag{2.50}$$

2.3 Reactions in Homogeneous Phase

In water treatment, gaseous chlorine Cl_2 or hypochlorite are commonly used for chlorination processes. Numerous inorganic and organic micro-pollutants can undergo reactions with chlorine. For most micro-pollutants, HOCl is the major reactive chlorine species during chlorination processes.

Chlorine reactivity usually results from an initial electrophilic attack of HOCl on inorganic and organic compounds. Oxidation, addition and electrophilic substitution reactions with organic compounds are possible pathways. However, from a kinetic point of view, usually only electrophilic attack is significant.

Under typical water treatment conditions in the pH range 6–9, hypochlorous acid and hypochlorite are the main chlorine species. Depending on the

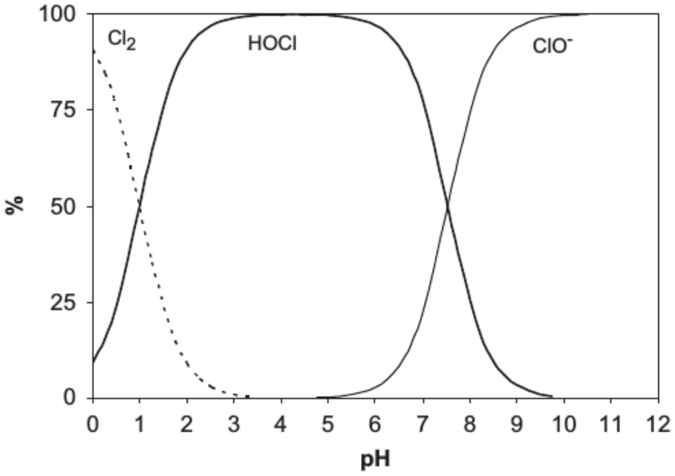

Figure 2.1: *Relative distribution of main aqueous chlorine species as a function of pH at 25 °C and for a chloride concentration of* $5 \cdot 10^{-3}$ *M.*

temperature and pH level, different distributions of aqueous chlorine species are observed. Figure 2.1 shows the distribution of Cl_2, HOCl and ClO^- as a function of the pH at 25 °C and for a chloride concentration of $5{\cdot}10^{-3}$ M. For high chloride concentrations, the Cl_2 hydrolysis is almost complete at pH >4. Therefore, Cl_2 can usually be neglected under typical drinking water treatment conditions. Most of HOCl is not ionized when pH is less than 7. If pH levels rise more than 8, most of the HOCl ionizes and more OCl^- is formed. The products of these reactions, Cl_2(aq), HOCl and OCl^- , are called "free available chlorine".

In this thesis, it is assumed that in the aqueous solution, chlorine Cl_2 is hydrolyzed to hypochlorous oxide HOCl, hypochlorous oxide dissociates into hypochlorous anion OCl^- and protons H^+ while water H_2O dissociates into protons and hydroxide OH^-.

The kinetics of Cl_2 hydrolysis is of importance in water chlorination treatment and in many reactions for both organic and inorganic constituents in water. Chlorine gas Cl_2 hydrolyzes in water according to the following reaction:

$$\mathrm{Cl_2 + H_2O \underset{k_{-1}}{\overset{k_1}{\rightleftharpoons}} HOCl + Cl^- + H^+}, \quad K_{\mathrm{Cl_2}} = k_1/k_{-1} \tag{2.51}$$

where $K_{\mathrm{Cl_2}}$ is the equilibrium constant and k_1=22.3 $\mathrm{s^{-1}}$ and k_{-1}=$4.3{\cdot}10^4$ $\mathrm{M^{-2}s^{-1}}$ are the forward and backward rate constants respectively. These values calculated[1] at I=0 M (ionic strength) and 25 °C.

Hypochlorous acid HOCl resulting from reaction (2.51), is a weak acid which dissociates in aqueous solution:

$$\mathrm{HOCl} \underset{k_{-1}}{\overset{k_1}{\rightleftharpoons}} \mathrm{ClO^-} + \mathrm{H^+}, \quad K_{\mathrm{HOCl}} \tag{2.52}$$

with K_{HOCl} reported in literature[2] $2.9{\cdot}10^{-8}$ ($\mathrm{pK}_{\mathrm{HOCl}_{25°C}}$=7.54) at 25 °C. Values for forward and backward reaction rates do not exist in the literature. Byrne et al. 2001 assumed a rate equal to that of water re-association. Although, in section 4.6, a different approach has been applied. The forward and backward reaction constants were chosen arbitrarily while keeping the restriction of a constant ratio equal to the equilibrium constant. In this way, the rate of the reaction was increased to a desired value.

For water dissociation, assuming that the applied electrical potential field does not affect the reaction rate, the reaction is:

$$\mathrm{H_2O} \underset{k_{-1}}{\overset{k_1}{\rightleftharpoons}} \mathrm{OH^-} + \mathrm{H^+} \tag{2.53}$$

where $k_1 = 2 \cdot 10^{-5}\ \mathrm{s}^{-1}$ and $k_{-1} = 1.11 \cdot 10^{8}\ \mathrm{m^3mol^{-1}s^{-1}}$ are the forward and backward rate constants[3], respectively.

---

[1] Wang and Margerum 1994

[2] Morris 1966

[3] Hlushkou, Crooks, and Tallarek 2009

Chapter 3

Mathematical Formulation

This chapter addresses the mathematical modeling of electrochemical systems from a macroscopic point of view.

In section 3.1, the governing equations for multi-ion transport in dilute electrolyte solutions is presented. The Poisson Equation and Electroneutrality condition are addressed in sections 3.2 and 3.3. The fundamental principle of charge conservation is specified in section 3.4. The flow of dilute electrolyte solutions is assumed to be governed by the incompressible Navier-Stokes and turbulent k-ϵ model equations, which are introduced in section 3.5. The present chapter concludes with the two mathematical models describing electrochemical systems in section 3.6.

3.1 Multi-Ion Transport in Dilute Electrolyte Solutions

In the following, a dilute electrolytic solution is considered which contains $m \geq 2$ different ionic species. For each ionic species $k = 1, ..., m$ present in the solution, the fundamental principle of mass conservation must hold. Mathematically this property is expressed as

$$\frac{d}{dt} \int_{V(t)} C_k d\mathbf{x} = - \int_{\partial V(t)} \mathbf{N}_i \cdot \mathbf{n} dS + \int_{V(t)} R_i d\mathbf{x} \tag{3.1}$$

where $\mathbf{N_i} \cdot \mathbf{n}$ the flux of ith species across the boundary $\partial V(t)$ and R_i a source or sink term.

The latter expression accounts for homogeneous chemical reactions within the volume, where ionic species i is either produced or consumed. As usual, $\mathbf{n}$ denotes the unit outer normal at the respective boundary part. The ionic flux due to diffusion (movement caused by concentration gradients), migration (movement caused by an electric field) and convection (movement caused by velocity) is given as

$$\mathbf{N_i} = (-\underbrace{D_i \nabla C_i}_{\text{Diffusion}} - \underbrace{z_i \mu_i F C_i \mathbf{E}}_{\text{Migration}} + \underbrace{\mathbf{u} C_i}_{\text{Convection}}) \tag{3.2}$$

In the literature, equation 3.2 is often referred as Nernst-Planck equation. Here, D_i is the molecular diffusion coefficient of species i with respect to the solute, z_i is the valence (charge number), μ_i the mobility constant, F Faraday's constant (96485.34 C/mol) and $\mathbf{E}$ the electric field inside the electrolyte solution.

Hence, the electric field vector is expressed in electrostatics as the negative gradient of the electrostatic potential field Φ reading,

$$\mathbf{E} = -\nabla \boldsymbol{\Phi} \tag{3.3}$$

As usual in dilute-solution theory, the mobility constant μ_i is assumed to be related to the diffusion coefficient D_i according to the Nernst-Einstein relation

$$\mu_i = \frac{D_i}{RT} \tag{3.4}$$

The relation involves the temperature T (specified in Kelvin (K)) and the universal gas constant R (8.314462 JK $^{-1}$ mol $^{-1}$).

Application of Reynold's transport theorem to the left-hand side of Equation 3.1 yields

$$\frac{d}{dt} \int_{V(t)} C_i d\mathbf{x} = \int_{V(t)} \frac{\partial C_i}{\partial t} d\mathbf{x} + \int_{\partial V(t)} C_i \mathbf{u} \cdot \mathbf{n} dS \tag{3.5}$$

The vector field $\mathbf{u}$ denotes the velocity of the electrolytic solution. Assuming sufficient smoothness of the respective functions, the divergence theorem (Gauss rule) is used to transform the boundary integrals in Equations 3.1 and 3.4 to integrals over the volume. As a result one obtains,

$$\int_{V(t)} (\frac{\partial C_i}{\partial t} + \nabla \cdot \mathbf{N_i} - R_i) d\mathbf{x} = 0 \tag{3.6}$$

Since relation 3.6 holds for every arbitrary reference volume $V(t)$, a partial differential equation is obtained for each ionic species $k = 1, ..., m$ present in the electrolytic solution, describing the temporal and spatial variation of its molar concentration C_i :

$$\frac{\partial C_i}{\partial t} + \nabla \cdot \mathbf{N_i} = R_i \tag{3.7}$$

3.2 Poisson Equation

For electrochemical systems, the electrostatic concept is commonly accepted as a sufficient modeling approach. For that case, the time-dependent coupling terms in the Maxwell equations vanish. As a consequence, electric and magnetic fields become decoupled, allowing a separate consideration of electro- and magnetostatics. The governing equations for electrostatics as obtained from Maxwell's equations read

$$\nabla \times \mathbf{E} = \mathbf{0} \tag{3.8}$$

$$\nabla \cdot \mathbf{D} = \rho_{\mathbf{e}} \tag{3.9}$$

Here, **D** denotes the so-called electric displacement field (C/m^2) and ρ_e is the net electric charge density (C/m^3). Since there are no free electrons in electrolyte solutions such as considered here, ions represent the only charge carriers. Thus, the local charge density is computed from the ionic concentrations C_i according to

$$\rho_e(\mathbf{x}, t) = F \sum_{i=1}^{m} z_i C_i(\mathbf{x}, t) \tag{3.10}$$

The electric displacement field **D** and the electric field **E** are related via a constitutive law, which is usually expressed in the form

$$\mathbf{D} = \epsilon \mathbf{E} \tag{3.11}$$

The permittivity ϵ (F/m) in 3.11 is a second-rank tensor reflecting individual material properties. For the most simple case of a homogeneous and isotropic medium, the permittivity is given as $\epsilon = \varepsilon_r \varepsilon_0 \mathbf{I}$, where ε_0 is the permittivity of the vacuum, ε_r denotes the medium-specific relative permittivity and **I** is the unit tensor.

A governing equation for the electric potential field is obtained by inserting Equation 3.10, 3.3 and 3.11 into 3.9. This yields the so-called Poisson equation for the electric potential:

$$-\nabla \cdot (\varepsilon \nabla \Phi) - F \sum_{i=1}^{m} z_i C_i = 0 \tag{3.12}$$

Although, assuming constant permittivity and locally electrically neutral electrolyte solution, the Equation 3.12 becoming a Laplace Equation

$$\nabla^2 \Phi = 0 \tag{3.13}$$

3.3 Electroneutrality condition

For macroscopic models, the system of equations is usually closed with the so-called electroneutrality condition instead of using 3.12. This condition is an algebraic constraint originating from the assumption that the electrolyte solution is locally electrically neutral:

$$\rho_e = F\sum_{i=1}^{m} z_i C_i = 0 \tag{3.14}$$

As pointed out by Newman and Thomas-Alyea 2004, the condition of electroneutrality is not a fundamental law of nature, but represents an "accurate approximation", which is generally accepted for a macroscopic description of electrochemical systems. Regions with considerable charge separation are solely the electric double layers in the vicinity of electrode-solution interfaces. A division of 3.14 by F transforms the electroneutrality condition into the form

$$\sum_{i=1}^{m} z_i C_i = 0 \tag{3.15}$$

which is usually used as closing equation.

3.4 Charge Conservation

A fundamental physical principle is charge conservation. Any modeling approach for electrochemical systems has to fulfill this elementary physical concept. The corresponding conservation law given, by direct consequence of the four Maxwell equations of electrodynamics, as

$$\frac{\partial \rho_e}{\partial t} + \nabla \cdot \mathbf{i} = \mathbf{0} \tag{3.16}$$

where ρ_e denotes the local net charge density in the medium and $\mathbf{i}$ is the local current density.
The current density depends on the ionic mass flux densities via

$$\mathbf{i} = F\sum_{i=1}^{m} z_i \mathbf{N}_i \tag{3.17}$$

since ions are both mass and charge carriers. The unit of the current density expressed in SI base units is A/m^2.

For ion-transport models coupled to the electroneutrality condition 3.15, $\rho_e \equiv 0$ in 3.16. In addition, convection does not contribute to the current density in 3.17 due to electroneutrality. Insertion of Nernst-Planck equation 3.2 of the ionic flux due to diffusion and migration into 3.2 yields

$$\begin{aligned}\mathbf{i} = F\sum_{i=1}^{m} z_i\mathbf{N}_i = F\sum_{i=1}^{m} z_i(-D_i\nabla C_i - z_i F\frac{D_i}{RT}C_i\nabla\Phi + \cancelto{\text{Electroneutrality}}{C_i\mathbf{u}}) &= \\ = -F\sum_{i=1}^{m} z_i D_i\nabla^2 C_i - F^2\sum_{i=1}^{m} z_i^2\frac{D_i}{RT}C_i\nabla^2\Phi &\end{aligned} \tag{3.18}$$

It is important to note that the concentration dependent factor in front of the gradient of the electric potential in 3.18 can be interpreted as a specific ionic conductivity of the electrolyte solution given as

$$\sigma = F^2\sum_{i=1}^{m} z_i^2\mu_i C_i = F^2\sum_{i=1}^{m} z_i^2\frac{D_i}{RT}C_i \tag{3.19}$$

As obvious from 3.19, local variations in the molar ion concentrations C_i, that is, variations in the electrolyte composition, will cause local variations in the ionic conductivity σ. In general, conductivity values are specified in the unit S/m. Thus, equation 3.18 is written,

$$\mathbf{i} = -F\sum_{i=1}^{m} z_i D_i\nabla C_i - \sigma\nabla\Phi \tag{3.20}$$

Finally, in the absent of space charge, equation 3.16 yields,

$$\begin{aligned}&\nabla\cdot\mathbf{i} = 0 \Leftrightarrow \\ \Leftrightarrow &\nabla\cdot(-F\sum_{i=1}^{m} z_i D_i\nabla C_i - \sigma\nabla\Phi) = 0\end{aligned} \tag{3.21}$$

3.5 Incompressible Flow

For dilute solutions, as considered here, concentrations of ionic species are very low compared to the solute. As a result, values for density and viscosity are typically similar to those of the pure solvent, but may depend on the local bath composition.

3.5.1 Laminar Flow

The steady-state equation for the motion of an incompressible Newtonian fluid is described by the Navier-Stokes and the continuity equation.

$$\rho(\mathbf{u} \cdot \nabla \mathbf{u}) = \nabla \bar{\sigma} + \mathbf{F} \quad (Navier - Stokes) \tag{3.22}$$

$$\rho(\nabla \mathbf{u}) = 0 \quad (Continuity) \tag{3.23}$$

where $\bar{\sigma}$ is the total stress tensor of the Newtonian fluid which consists of pressure stress and viscous stress

$$\bar{\sigma} = -p\mathbf{I} + \mu(\nabla \mathbf{u} + (\nabla \mathbf{u})^T) \tag{3.24}$$

Here **u** is the fluid velocity vector, ρ the fluid density, **F** is the body force or volumetric force, **I** is the identity tensor.
The boundary conditions are described in Table 3.1.

Table 3.1: *Boundary conditions in case of laminar flow using Navier-Stokes equation.*

Boundary	**Boundary Condition**	**Equation**
Wall	No-slip	$\mathbf{u} = 0$
Fluid Inlet	Velocity	$\mathbf{u} = -u_0\mathbf{n}$
Fluid Outlet	Pressure	$p = p_0$
Symmetry	Symmetry Condition	$\mathbf{u} \cdot \mathbf{n} = 0$

3.5.2 Turbulent Flow

Two types of turbulence energy equation models are One-Equation Models and Two-Equation Models both retain the Boussinesq eddy-viscosity approximation[1] but differ in one important respect. Two-Equation models provide an equation for the turbulence length scale or its equivalent and are thus complete.

In the framework of eddy viscosity models, the steady state flow of a turbulent incompressible fluid is governed by the RANS equations for the velocity vector **u** and pressure p.

$$\begin{aligned} &\rho(\mathbf{u} \cdot \nabla \mathbf{u}) = -\nabla p + \nabla \cdot ((\mu + \mu_T)[\nabla \mathbf{u} + \nabla \mathbf{u}^T]) \\ &\nabla \cdot \mathbf{u} = 0 \end{aligned} \tag{3.25}$$

---

[1] In 1887 Boussinesq proposed relating the turbulence stresses to the mean flow to close the system of equations

where viscosity μ depends only on the physical properties of the fluid, while μ_T is the turbulent eddy viscosity which is supposed to emulate the effect of unresolved velocity vector fluctuations $\mathbf{u}'$.

By far, the most popular Two-Equation model is the k-ϵ model. The standard k-ϵ model is based on the assumption that

$$\mu_T = \rho C_\mu \frac{k^2}{\epsilon} \tag{3.26}$$

where k is the turbulent kinetic energy (half the trace of the Reynolds stress tensor),

$$k = \frac{1}{2}\rho\overline{u'_i u'_i} \tag{3.27}$$

and ϵ is the dissipation rate. Hence, the above PDE system (3.25) is to be complemented by two additional convection-diffusion-reaction equations for computation of k and ϵ.

$$\begin{aligned} \rho(\mathbf{u}\cdot\nabla k) &= \nabla\cdot((\mu + \frac{\mu_T}{\sigma_k})\nabla k) + P_k - \rho\epsilon \\ \rho(\mathbf{u}\cdot\nabla \epsilon) &= \nabla\cdot((\mu + \frac{\mu_T}{\sigma_\epsilon})\nabla \epsilon) + C_{\epsilon 1}\frac{\epsilon}{k}P_k - C_{\epsilon 2}\rho\frac{\epsilon^2}{k} \end{aligned} \tag{3.28}$$

where P_k

$$P_k = \mu_T[\nabla\mathbf{u}(\nabla\mathbf{u} + (\nabla\mathbf{u})^T)] \tag{3.29}$$

and ϵ are responsible for the production and dissipation of the turbulent kinetic energy, respectively. The default values of the involved empirical constants are

$$C_\mu = 0.09, \quad C_{\epsilon 1} = 1.44, \quad C_{\epsilon 2} = 1.92, \quad \sigma_k = 1.0, \quad \sigma_\epsilon = 1.3 \tag{3.30}$$

The boundary conditions in the case of the turbulent k-ϵ model are:

Wall Functions

$$\begin{aligned} &\mathbf{u}\cdot\mathbf{n} = 0 \\ &[(\mu + \mu_T)(\nabla\mathbf{u} + (\nabla\mathbf{u})^T) - \frac{2}{3}\rho k\mathbf{I}]\mathbf{n} = -\rho\frac{u_\tau}{\delta_w^+}(\mathbf{u} - (\mathbf{u}\cdot\mathbf{n})\mathbf{n}) \\ &\nabla k\cdot\mathbf{n} = 0, \quad \epsilon = \rho\frac{C_{mu}k^2}{\kappa_v\delta_w^+\mu} \end{aligned} \tag{3.31}$$

Fluid Inlet

$$\begin{gathered}\mathbf{u} = -u_0\mathbf{n} \\ k = \frac{3}{2}(u_0 I_T)^2, \quad \epsilon = C_\mu^{3/4}\frac{k^{3/2}}{L_T}\end{gathered} \tag{3.32}$$

Fluid Outlet

$$\begin{aligned}&[-p\mathbf{I} + (\mu + \mu_T)(\nabla\mathbf{u} + (\nabla\mathbf{u})^T) - \frac{2}{3}\rho k\mathbf{I}]\mathbf{n} = -p_0\mathbf{n} \\ &\nabla k \cdot \mathbf{n} = 0, \quad \nabla\epsilon \cdot \mathbf{n} = 0\end{aligned} \tag{3.33}$$

Symmetry Condition

$$\mathbf{u} \cdot \mathbf{n} = \mathbf{0} \tag{3.34}$$

3.6 Mathematical Models

3.6.1 Secondary Current Distribution

The Secondary Current Distribution model calculates the electrolyte potential without taking into consideration the diffusion term:

$$\mathbf{i} = -\sigma\nabla\Phi \tag{3.35}$$

In this case, the charge conservation equation (3.16), in the absence of space charge, is expressed as:

$$\begin{gathered}\nabla \cdot \mathbf{i} = 0 \Leftrightarrow \\ \Leftrightarrow \nabla \cdot (-\sigma\nabla\Phi) = 0\end{gathered} \tag{3.36}$$

This model is not concentration dependent. Thus, in order to add concentration variables into the system, Equation 3.36 can be coupled with Equation 3.7

$$\frac{\partial C_i}{\partial t} + \nabla \cdot \mathbf{N_i} = \mathbf{R_i} \tag{3.37}$$

where C_i is the concentration of ith species, R_i the reaction rate in the homogeneous phase of the electrolyte of the ith species and $\mathbf{N_i}$ the Nernst-Planck's flux of the ith species (Equation 3.2):

$$\mathbf{N_i} = (-\underbrace{D_i\nabla C_i}_{\text{Diffusion}} - \underbrace{z_i\mu_i F C_i\mathbf{E}}_{\text{Migration}} + \underbrace{\mathbf{u}C_i}_{\text{Convection}}) \tag{3.38}$$

where the velocity $\mathbf{u}$ can be obtained by one of the models described in section 3.5 depending if the incompressible flow is considered laminar or turbulent. The boundary conditions of these two coupled models, Secondary Current Distribution and Multi-ion Transport in Dilute Electrolyte Solutions can be seen in Tables 3.3 and 3.2.

Table 3.2: *Boundary conditions in case of Secondary Current Distribution model.*

Boundary	**Boundary Condition**	**Equation**
Electrodes	Feeder Electrodes	$-\mathbf{n}\cdot\mathbf{i_l} = i_{total} = \sum_{m}^{\text{Redox}} i_{loc,m}$
	Bipolar Electrodes	$-\mathbf{n}\cdot\mathbf{i_l} = i_{total} = \sum_{m}^{\text{Redox}} i_{loc,m} = -\mathbf{n}\cdot\mathbf{i_s}$
Walls	Insulators	$-\mathbf{n}\cdot\mathbf{i_l} = 0$
Inlet & Outlet	Insulators	$-\mathbf{n}\cdot\mathbf{i_l} = 0$
Symmetry	Symm. Condition	$-\mathbf{n}\cdot\mathbf{i_l} = 0, \quad -\mathbf{n}\cdot\mathbf{i_s} = 0$

Table 3.3: *Boundary conditions in case of Multi-ion Transport in Dilute Electrolyte Solutions.*

Boundary	**Boundary Condition**	**Equation**
Electrodes	Feeder & Bipolar El.	$-\mathbf{n}\cdot\mathbf{N_i} = \sum_{m}^{\text{Redox}} (\frac{v_i i_{loc_m}}{n_m F})_{\mathrm{m}}$
Walls	No flux	$-\mathbf{n}\cdot\mathbf{N_i} = 0$
Inlet	Concentration	$c_i = c_{0i}$
Outlet	Concentration Grad.	$-\mathbf{n}\cdot\mathbf{D_i}\nabla\mathbf{c_i} = \mathbf{0}$
Symmetry	No flux	$-\mathbf{n}\cdot\mathbf{N_i} = \mathbf{0}$

It is worth mentioning that the model presented here can be implemented in COMSOL by coupling the "Secondary Current Distribution" and "Transport of Diluted Species" modules.

3.6.2 Tertiary Current Distribution

Tertiary Current Distribution is a complete concentration dependent model. The electrolyte current density is expressed as equation 3.20

$$\mathbf{i} = -F\sum_{i=1}^{m} z_i D_i \nabla C_i - \sigma\nabla\Phi \tag{3.39}$$

where electroneutrality condition (equation 3.15) is taken into account,

$$\sum_{i=1}^{m} z_i C_i = 0 \tag{3.40}$$

Therefore, the charge conservation equation (3.16), in the absence of space charge, is expressed as in equation 3.18:

$$\begin{aligned} &\nabla \cdot \mathbf{i} = 0 \Leftrightarrow \\ \Leftrightarrow &- F \sum_{i=1}^{m} z_i D_i \nabla^2 C_i - F^2 \sum_{i=1}^{m} z_i^2 \frac{D_i}{RT} C_i \nabla^2 \Phi = 0 \end{aligned} \tag{3.41}$$

Furthermore, the mass conservation equation holds:

$$\frac{\partial C_i}{\partial t} + \nabla \cdot \mathbf{N_i} = \mathbf{R_i} \tag{3.42}$$

where $\mathbf{N_i}$

$$\mathbf{N_i} = (- \underbrace{D_i \nabla C_i}_{\text{Diffusion}} - \underbrace{z_i \mu_i F C_i \mathbf{E}}_{\text{Migration}} + \underbrace{\mathbf{u} C_i}_{\text{Convection}}) \tag{3.43}$$

where the velocity $\mathbf{u}$ can be obtained by one of the models described in section 3.5 depending if the incompressible flow is considered laminar or turbulent. Finally, the boundary conditions are the same as in Tables 3.3 and3.2.

Chapter 4

Computational Approach

This chapter presents a summary of the examined cases concerning the modeling of the electrochemical reactor, carried out by using the COMSOL Multiphysics software.

In sections 4.1, 4.2 and 4.3 different reactor geometries, by changing electrodes configuration, will be examined under the same operating conditions using a laminar flow (inlet velocity 0.05 m/s) .

In section 4.4 a comparison between the two mathematical models (Secondary and Tertiary described in Chapter 3) will be made under the same operating conditions in the reactor of geometry I using a laminar flow (inlet velocity 0.05 m/s).

In section 4.5, the effect of changing the value of the inlet velocity from 0.05 m/s (laminar flow) to 1.5 m/s (turbulent flow) will be presented. The two models will be compared under same operating conditions in the reactor of geometry I.

In section 4.6, the effect of the reactions in the homogeneous phase (electrolyte) will be presented using turbulent flow (inlet velocity 1.5 m/s) in the reactor of geometry I.

Finally, in section 4.7, the modeling of a complete reactor with 5 bipolars will be examined. Also, different electrode reaction rates of O_2 production will be presented.

On the one hand, when Tertiary Current Distribution mathematical model is used, COMSOL's "Tertiary Current Density, Nernst-Planck" module is implemented. This module includes both potential and concentration variables. On the other hand when Secondary Current Distribution mathematical model is used, COMSOL's "Secondary Current Density" module, which calculates the potential variable (both electrolyte and bipolar electrode), has to be coupled with COMSOL's "Transport of Diluted Species" module in order to add the calculation of concentration variables. In the second case, the coupling of the two modules achieved due to the presence of the electrolyte potential variable in both modules.

In the two aforementioned cases the calculation of the velocity variable comes separately from the calculation of potentials (bipolar electrode's and electrolyte's) and concentration variables.

In the case where a Secondary Current Distribution model is used, then three modules have been applied in COMSOL:

a. Single-Phase Flow
    - Laminar Flow or
    - Turbulent Flow,k-ϵ

b. Transport of Diluted Species

c. Secondary Current Distribution

where the Single Phase flow is solved independently while the Secondary Current Distribution is coupled with Transport of Diluted Species

In the case where a Tertiary model is used then two modules have been applied:

a. Single Phase Flow
    - Laminar Flow or
    - Turbulent Flow,k-ϵ

b. Tertiary Current Distribution, Nernst-Planck

In all cases, the Secondary Current Distribution mathematical model (as described in section 3.6.1) will be used except of the case (in section 4.4) where both Tertiary and Secondary Current Density models are compared.

In all examined cases, water (electrolytic solution) enters the reactor at temperature 298.15 K and pH 7.5. The inlet concentration of chlorides Cl^- is 1660 mg/L. The concentration of Sodium Na^+ at the inlet is calculated in such way to enforce electroneutrality condition. The diffusion coefficients for Cl^-, Na^+, H^+ and OH^- are taken from Nguyen 2008, diffusion coefficient for Cl_2 from Vasconcelos and Boulos 1996 and diffusion coefficient for OCl^- and HOCl from Byrne 2001. Although, HOCl and OCl^- species are included only in the case of 4.6.

The inlet concentrations and diffusion coefficients for Cl^-, Na^+, H^+, OH^-, Cl_2, HOCl and OCl^- can be seen in Table 4.1.

Table 4.1: *Inlet concentrations and diffusion coefficients for* Cl^-, Na^+, H^+, OH^-, Cl_2, *HOCl and* OCl^-.

Species	**Concentration (mol/m^3)**	**Diffusion Coefficient (m^2/s)**
Cl^-	46.8	$2.03 \cdot 10^{-9}$
Na^+	46.8003	$1.33 \cdot 10^{-9}$
H^+	$3.16228 \cdot 10^{-5}$	$9.31 \cdot 10^{-9}$
OH^-	$3.16228 \cdot 10^{-4}$	$5.28 \cdot 10^{-9}$
Cl_2	0	$1.25 \cdot 10^{-9}$
HOCl	0	$1.11 \cdot 10^{-9}$
OCl^-	0	$1.07 \cdot 10^{-9}$

Furthermore, in all cases the electrode reactions producing Cl_2 and O_2 are of the form of Equations 2.15 and 2.49

$$i = Fk_2 \frac{k_1}{k_{-1}} e^{2\frac{F}{RT}E^\circ} (C_{\mathrm{Cl^-}})^2 e^{2\frac{F}{RT}(E-E^\circ)} - Fk_{-2}C_{\mathrm{Cl_2}}$$

$$i = i_0 e^{0.5\frac{F}{RT}(E-E_{\mathrm{eq}})}$$

Although, in the case of section 4.7 another O_2 evolution reaction is examined which has the form of Equation 2.46

$$i = i_0 \frac{C^*_{\mathrm{H^+}}}{C_{\mathrm{H^+}}} e^{1.5\frac{F}{RT}(E-E_{\mathrm{eq}})}$$

Also, for all the examined cases, the H_2 evolution reaction is:

$$i = -i_0 e^{0.5\frac{F}{RT}(E-E_{\mathrm{eq}})} \tag{4.1}$$

Reaction 4.1 results from Volmer-Heyrovsky pathway with the Volmer step as rate determining while taking into account only the cathodic term. The kinetic parameters of the above reactions can be seen in Table 4.2.

When Secondary C.D. model is used, the electrolyte conductivity is constant 0.59053 S/m calculated from equation 3.19 using the inlet concentrations of species.

In case of laminar flow, the COMSOL's "Laminar Flow" module is used and it is assumed inlet velocity of 0.05 m/s, also zero pressure is assumed at the outlet. On the contrary, when the inlet velocity is 1.5 m/s (turbulent flow) then COMSOL's "Turbulent Flow,k-ϵ" module is used. In this case, boundary conditions at the inlet it is assumed 0.05 turbulent intensity[1] and

---

[1] `http://www.comsol.com/model/download/184799/models.cfd.water_purification_reactor.pdf`

Table 4.2: *Kinetic parameters for electrode reactions of Cl_2, $O_2$and H_2 production.*

Kinetic Parameters	**Values**
$i_{0\mathrm{Cl_2}}$	1 A/m^2
$i_{0\mathrm{O_2}}$	$2\cdot 10^{-6}$ A/m^2
$i_{0\mathrm{H_2}}$	$1\cdot 10^{-3}$ A/m^2
$E_{\mathrm{eqH_2}}$	-0.44316 V
$E_{\mathrm{eqO_2}}$	0.75330 V
$E^{\circ}_{\mathrm{Cl_2}}$	1.36 V

0.9366 mm turbulence length scale.[1] Also, zero pressure is assumed at the outlet.

In most of the cases finding appropriate initial values for the system to converge was a difficult task. Therefore, downgrading the problem to a simpler problem, e.g simpler electrode reactions or slower reaction kinetics in homogeneous phase, has been proved a very convenient method. In addition, implementing a transient solver for a couple of either seconds or minutes gave good convergence (not always) but it was a very time consuming method.

In some cases the presence of negative concentrations changed significantly the expected results. In order to overcome that obstacle, a segregated solver instead of a fully coupled solver has been preferred.

The mesh used in the examined cases, was created by COMSOL's mesh generator. The mesh consists of unstructured triangular mesh along with quadrilateral elements (for boundary layer mesh) because of fluid flow. Due to the exponent in the electrode reactions's boundary condition, an extra mesh refinement in the edges of electrodes is needed. Although, this increases the number of mesh elements. Also, when the number of mesh's boundary layers on boundaries is increased, it leads to worst average element quality. Furthermore, increasing the total number of elements leads to an increase of computational time.

As a result of the above comments, the properties of the mesh are shown in Table 4.3. In most of the examined cases, mesh properties were kept the same. Nevertheless, in sections 4.3 and 4.7 these properties were reduced to a more coarse mesh.

---

[1] Turbulence Length Scale = 0.07·(Characteristic Length) [*Comsol, User's Guide* 2012]

Table 4.3: *Mesh properties for the examined cases.*

Mesh Properties	
Calibrate for	Fluid Dynamics, Finer
Boundaries	Extra Fine
Domain	Finer
Corner Refinement	0.25
Number of Boundary Layers	2

4.1 Geometry I

Figure 4.1 depicts a very simple configuration of four, in total, feeder electrodes and two bipolar electrodes. Applying the mesh properties, as described in Table 4.3, the resulting mesh for this geometry, consists of 69868 elements with average element quality 0.914. In Figure 4.2 it is apparent that the potential of feeder electrodes is given as a Dirichlet Boundary Condition (Figure 4.2a) while for the bipolar electrode the potential is calculated, as can be seen by the presence of a mesh within it (Figure 4.2b).

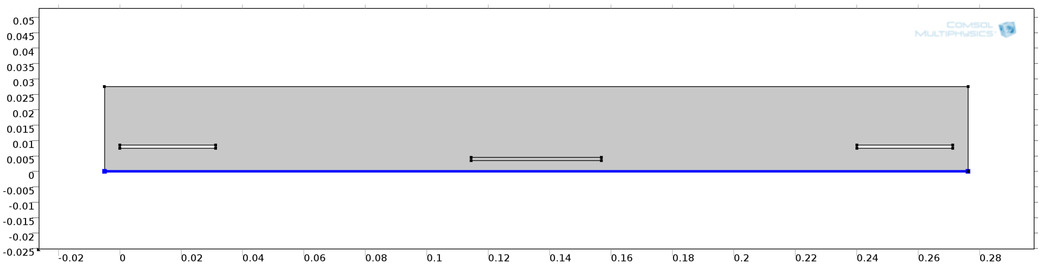
0.05
0.045
0.04
0.035
0.03
0.025
0.02
0.015
0.01
0.005
0
-0.005
-0.01
-0.015
-0.02
-0.025
-0.02
0
0.02
0.04
0.06
0.08
0.1
0.12
0.14
0.16
0.18
0.2
0.22
0.24
0.26
0.28

Figure 4.1: *Geometry I with four feeder electrodes (anode on the left and cathode on the right) and two bipolar electrodes (in the middle). Blue axis denotes symmetry plane*

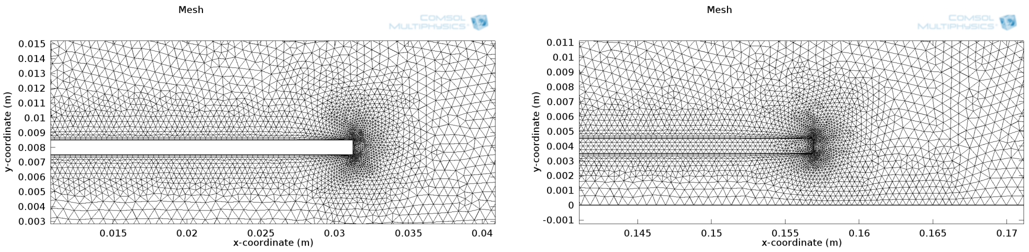
Mesh
y-coordinate (m)
0.015
0.014
0.013
0.012
0.011
0.01
0.009
0.008
0.007
0.006
0.005
0.004
0.003
0.015
0.02
0.025
0.03
0.035
0.04
x-coordinate (m)
Mesh
y-coordinate (m)
0.011
0.01
0.009
0.008
0.007
0.006
0.005
0.004
0.003
0.002
0.001
0
-0.001
0.145
0.15
0.155
0.16
0.165
0.17
x-coordinate (m)

(a) *Anode feeder electrode* (b) *Bipolar electrode*

Figure 4.2: *Unstructured triangular mesh with boundary layer quadrilateral elements.*

The flow is considered laminar with inlet velocity 0.05 m/s. The Laminar Flow module solved 110490 degrees of freedom. The distribution of the velocity magnitude can be seen in Figure 4.3. The coupling between Secondary Current Distribution module and Transport of Diluted Species modules solved 221781 degrees of freedom (plus 12732 internal DOFs).

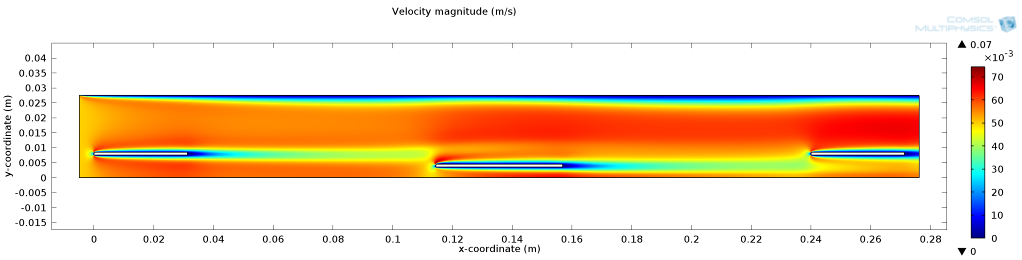

Figure 4.3: *Velocity magnitude distribution of Geometry I.*

Applying 10 V in feeder electrodes, with electrode reactions those described in the beginning of this chapter, the electrolyte potential distribution and the contour of the y-component of the electrolyte current density vector are shown in Figure 4.4. The potential of the bipolar electrode has a homogeneous distribution of 5.07 V.

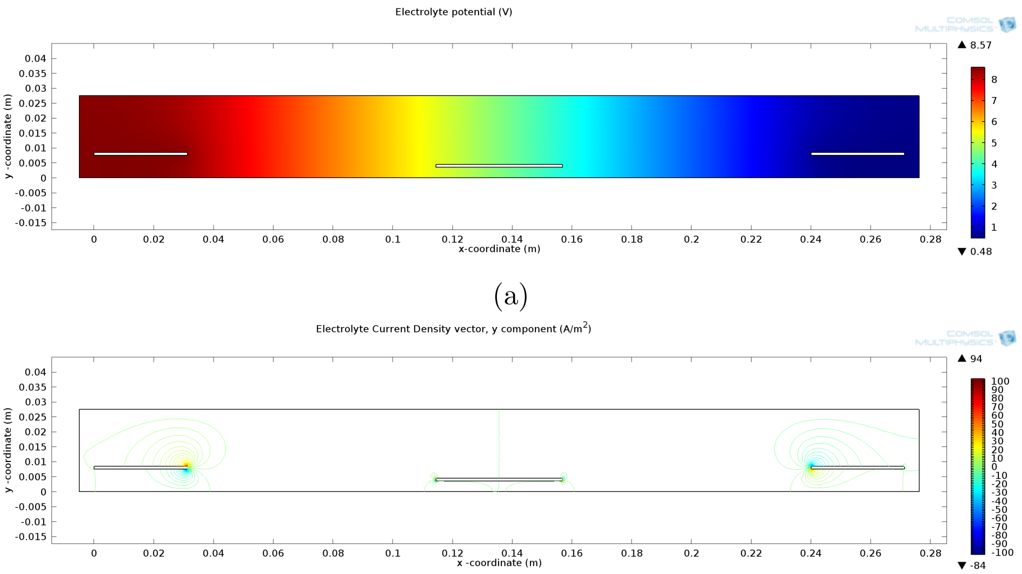

(a)

(b)

Figure 4.4: *Applied potential 10 V in Geometry I:* ***a)*** *Electrolyte potential distribution and* ***b)*** *Electrolyte current density vector, y-component.*

As can be seen in Figure 4.4b, the bipolar electrode behaves as an insulator due to the absence of y-component electrolyte current density vector connected on the horizontal edges. Moreover, the local current density produced on the bipolar electrode was very small as a result of the low overpotentials (Figure 4.5).

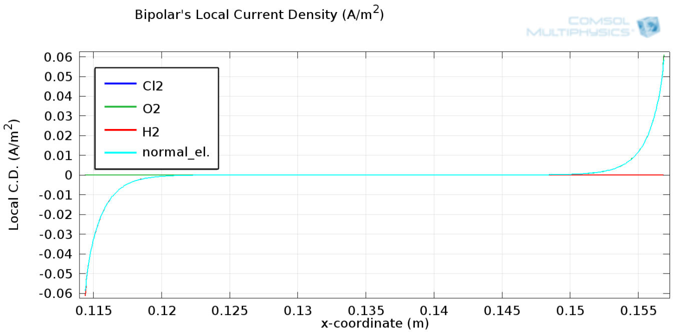

(a)

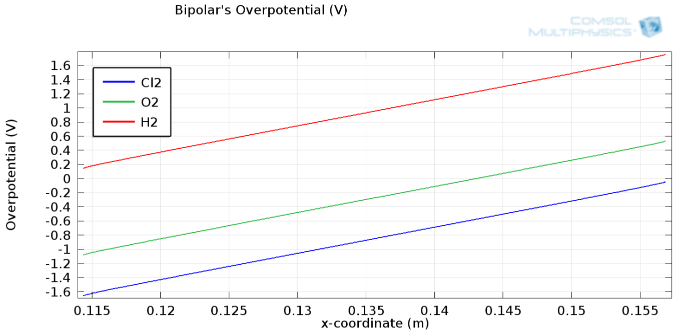

(b)

Figure 4.5: *Applied potential 10 V in Geometry I on the upper horizontal side of bipolar electrode:* ***a)*** *Local current density of the reactions producing* Cl_2*,* O_2 *and* H_2 *also the normal vector of electrolyte current density is plotted and* ***b)****Overpotential of the aforementioned reactions.*

Since the voltage of 10 V was not sufficient to make the conductive body behaving as a bipolar electrode, it was raised to 30 V. In this case, as can be seen in Figure 4.6, the conductive body behaves as desired (cathode on the left side and anode on the right side).

The local current density on the bipolar electrode has high values because of the high overpotential (Figure 4.7)

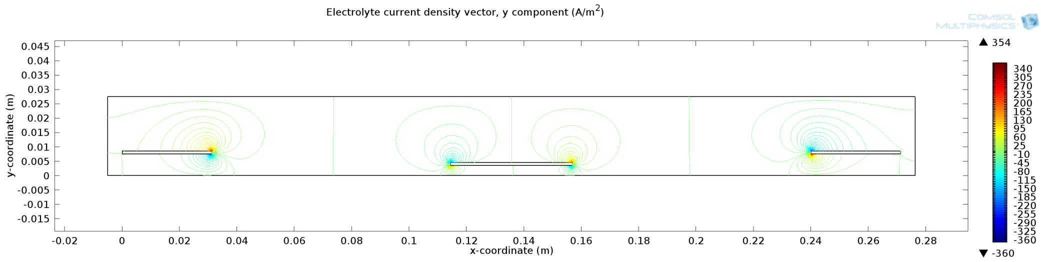

Figure 4.6: *Electrolyte current density vector, y-component of Geometry I for applied potential 30 V.*

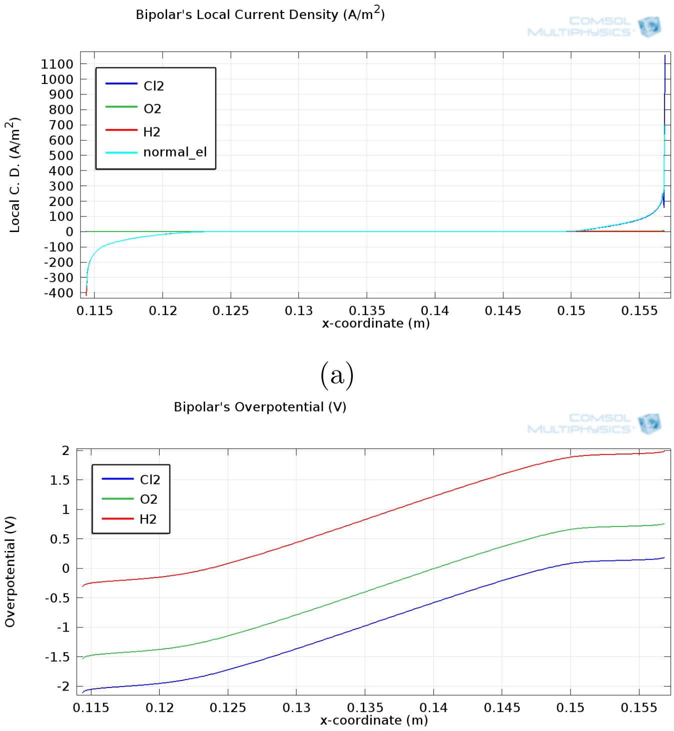

(a)

(b)

Figure 4.7: *Applied potential 30 V in Geometry I on the upper horizontal side of bipolar electrode:* ***a)*** *Local current density of the reactions producing Cl_2, O_2 and H_2 also the normal vector of electrolyte current density is plotted and* ***b)****Overpotential of the aforementioned reactions.*

4.2 Geometry II

In section 4.1 changing the applied voltage of the feeder electrodes resulted in a vast difference in the behavior of the system. In this section, all operating conditions are kept the same (as in geometry I) with 10 V applied voltage but the horizontal distance of the electrodes will be changed. Geometry II depicts a reactor with four, in total, feeder electrodes and two bipolar electrodes but in a closer distance (Figure 4.9).

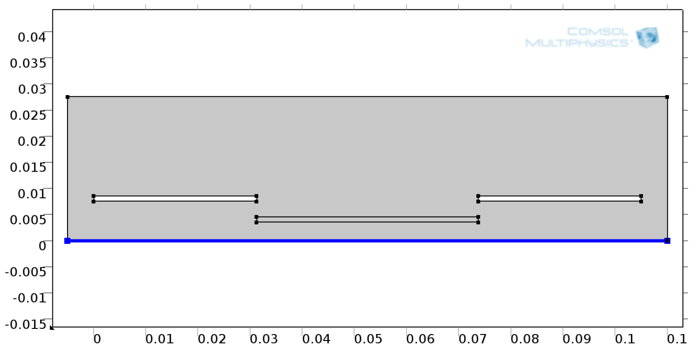

Figure 4.8: *Geometry II with four feeder electrodes (anode on the left and cathode on the right) and two bipolar electrodes (in the middle). Blue axis denotes symmetry plane*

Applying the mesh properties, as described in the beginning of the current chapter (Table 4.3), the resulting mesh, for this geometry, consists of 39201 elements with average element quality 0.914.

The flow is considered laminar with inlet velocity 0.05 m/s. The Laminar module solved 62175 degrees of freedom. The distribution of the velocity magnitude is presented in Figure 4.9.

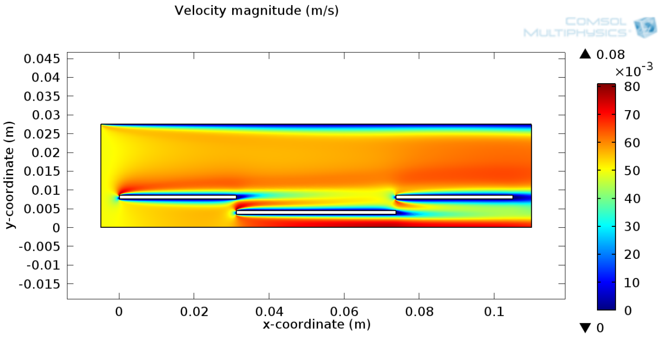

Figure 4.9: *Velocity magnitude distribution of Geometry II.*

The coupling between Secondary Current Distribution module and Transport of Diluted Species modules solved 125147 degrees of freedom (plus 8574 internal DOFs). The resulting electrolyte potential distribution and the contour of the y-component of the electrolyte current density vector are shown in Figure 4.10. The potential of the bipolar electrode has a homogeneous distribution of 5.07 V.

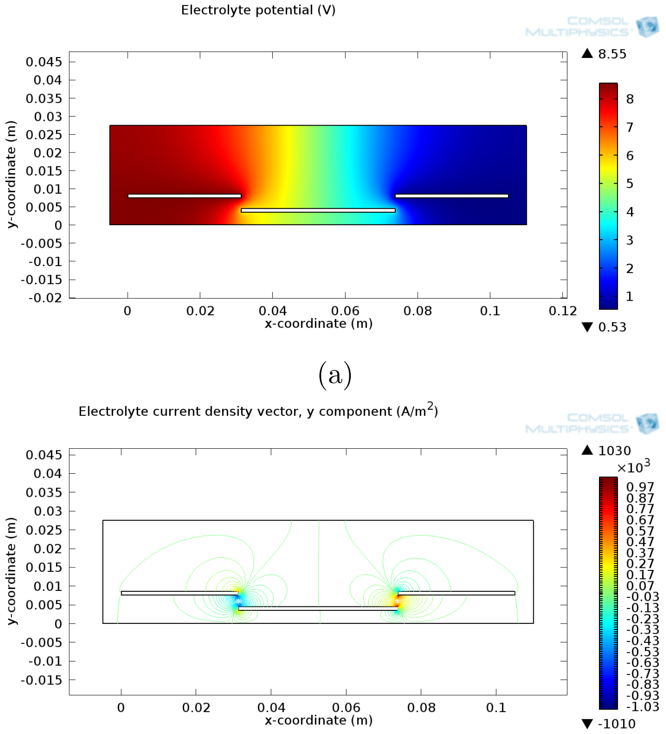

(a)

(b)

Figure 4.10: *Applied potential 10 V in Geometry II:* ***a)*** *Electrolyte potential distribution and* ***b)*** *Electrolyte current density vector, y-component.*

As can be seen in Figure 4.10b, the conductive body not only behaves as expected (bipolar electrode) but a bigger fraction of the surface is active, thus producing current. This observation can be confirmed by plotting the local current density of all electrode reactions on the upper side of the bipolar electrode in Figure 4.11 where overpotentials give high values not only on the edges but in the inner parts as well.

Finally, the configuration of the electrodes in Geometry II, provokes an increase of the produced chlorine in the outlet of the reactor compared to Geometry I (Figure 4.12).

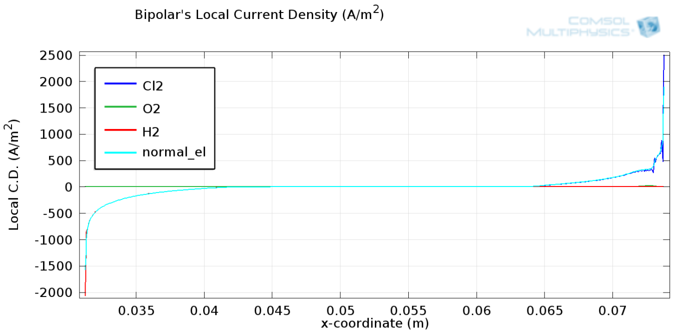

(a)

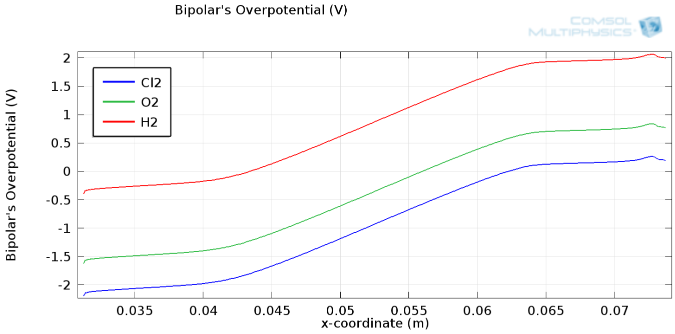

(b)

Figure 4.11: *Applied potential 10 V in Geometry II on the upper horizontal side of bipolar electrode:* ***a)*** *Local current density of the reactions producing Cl_2, O_2 and H_2 also the normal vector of electrolyte current density is plotted and* ***b)*** *Overpotential of the aforementioned reactions.*

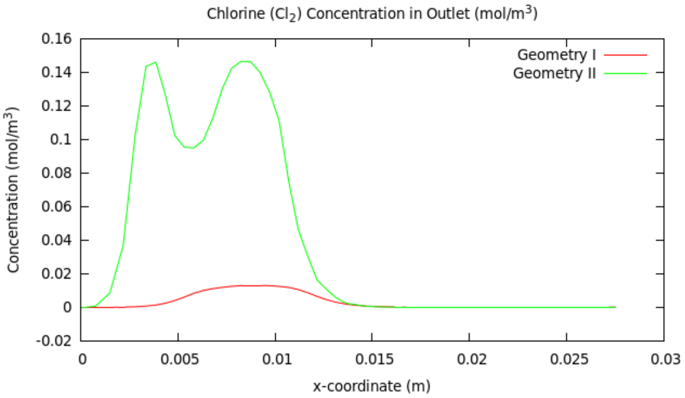

Figure 4.12: *Chlorine Cl_2 concentration (mol/m_3) in the outlet of the reactor of Geometry I and Geometry II*

4.3 Geometry III

In section 4.2 the change in geometry produced high currents on the bipolar electrodes. In this section the configuration of the electrodes will be further changed to resemble the configuration of the reactor (Figure 1.1). Figure 4.13 depicts geometry III with four, in total, feeder electrodes and two bipolar electrodes.

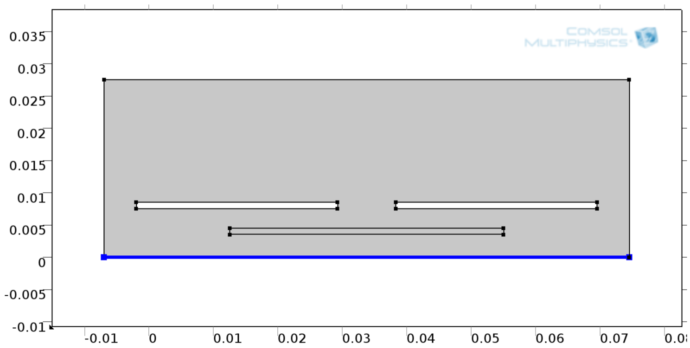

Figure 4.13: *Geometry III with four feeder electrodes (anode on the left and cathode on the right) and two bipolar electrodes (in the middle). Blue axis denotes symmetry plane*

Due to convergence difficulties of this geometry, different mesh properties, have been chosen (Table 4.4). The resulting coarser mesh of the geometry III consists of 7071 elements with average element quality 0.8482. The flow is considered laminar with inlet velocity 0.05 m/s. The Laminar Flow module solved 12120 degrees of freedom. The distribution of the velocity magnitude is shown in Figure 4.14.

Table 4.4: *Mesh properties for the examined case.*

Mesh Properties	
Calibrate for	Fluid Dynamics, Normal
Boundaries	Fine
Domain	Coarse
Corner Refinement	0.25
Number of Boundary Layers	2

The coupling between Secondary Current Distribution module and Transport of Diluted Species modules solved 24446 degrees of freedom (plus 3405 internal DOFs). The resulting electrolyte potential distribution and the contour of the y-component of the electrolyte current density vector are shown in

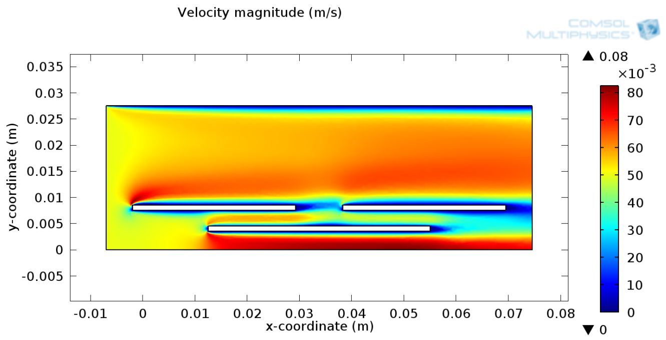

Figure 4.14: *Velocity magnitude distribution of Geometry III.*

Figure 4.15. Also, the potential of the bipolar electrode has a homogeneous distribution of 5 V.

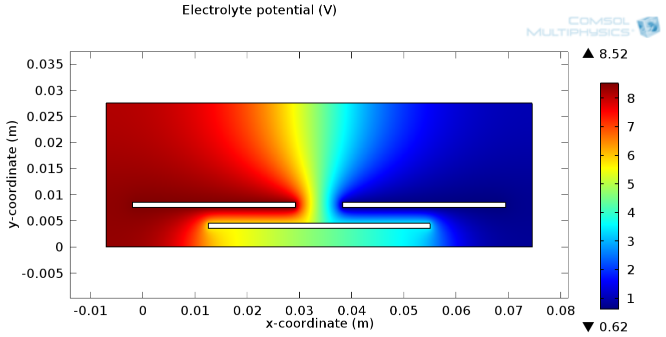

(a)

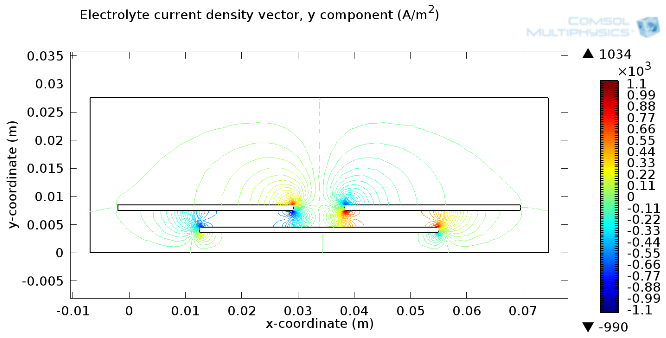

(b)

Figure 4.15: *Applied 10 V in Geometry III:* ***a)*** *Electrolyte potential distribution and* ***b)*** *Electrolyte current density vector, y-component.*

The contour lines of the y-component of the electrolyte current density, in Figure 4.15b, are present throughout the bipolar electrode. This observation is confirmed by plotting the local current distribution on the conductive body (Figure 4.16a).

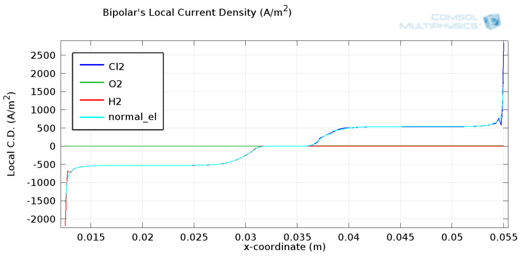

(a)

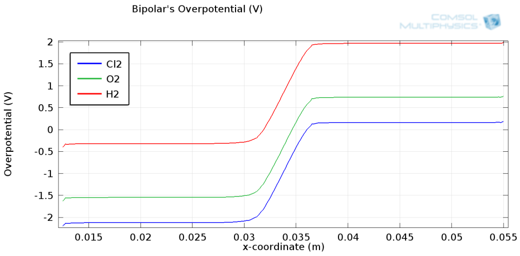

(b)

Figure 4.16: *Applied 10 V in Geometry III on the upper horizontal side of bipolar electrode:* ***a)*** *Local current density of the reactions producing Cl_2, O_2 and H_2 also the normal vector of electrolyte current density is plotted and* ***b)****Overpotential of the aforementioned reactions.*

Finally, the configuration of the electrodes in Geometry III, provokes an increase of the produced chlorine in the outlet of the reactor compared to Geometry I and Geometry II (Figure 4.17).

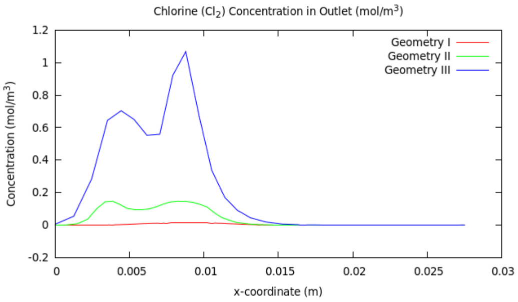

Figure 4.17: *Chlorine Cl_2 concentration (mol/m_3) in the outlet of the reactor of Geometry I, Geometry II and Geometry III*

4.4 Geometry I with Secondary and Tertiary Models

In this section a comparison between two mathematical models will be made via COMSOL's modules. On the one hand there is the Secondary Current Distribution coupled with Transport of Diluted species module and on the other hand the Tertiary Current Distribution module. The comparison will be implemented in the Geometry I applying 10 V, using laminar flow of inlet velocity 0.05 m/s. Under these operating conditions the Secondary Current Distribution module was presented in section 4.1. The choice of 10 V applied voltage, where the conductive body didn't behave as bipolar, was made in order to test if the Tertiary model will reveal or not the same behavior.

Applying the mesh properties, as described in the beginning of the current chapter, the resulting mesh is identical to those of section 4.1 (69868 total elements with average element quality 0.914). There is a big difference in the number of degrees of freedom solved for the two models. Tertiary model needed 727151 degrees of freedom (plus 20940 internal DOFs) while Secondary coupled with Transport needed 221781 DOFs (plus 12732 internal DOFs).

The Laminar Flow module is been solved independently so that the velocity distribution is identical to this of section 4.1. Solving the Tertiary module, the electrolyte potential distribution is obtained which is identical to that of the Secondary module, as can be seen in Figure 4.18. Also, the bipolar potential is of the same value (5.07 V) between the two models.

The produced currents on the upper side of the electrodes (both feeders and bipolar) were almost identical between the two models (Figure 4.19).

The fact that the currents on the electrode's faces were almost identical, can be explained by the fact that the electrolyte and bipolar potentials were also identical. Moreover, the concentrations of chlorine (Cl_2), hydrogen ion (H^+), chloride ion (Cl^-) and hydroxide (OH^-), which affect electrode's reactions are also similar between the two models. Only, concentrations of chlorine (Cl_2) and chloride ion (Cl^-) on the upper side of anode present a small difference as, can be seen in Figure 4.20.

Nevertheless, in the homogeneous phase (electrolyte) there was a significant deviation of concentration values of the produced species Cl_2, OH^- and H^+, between the two models. Figure 4.21 shows this difference along the reactor (at height of 0.006 m). This fact was expected since the electroneutrality condition has been taken into account in the Tertiary model. The deviation from electroneutrality condition of the Secondary model can

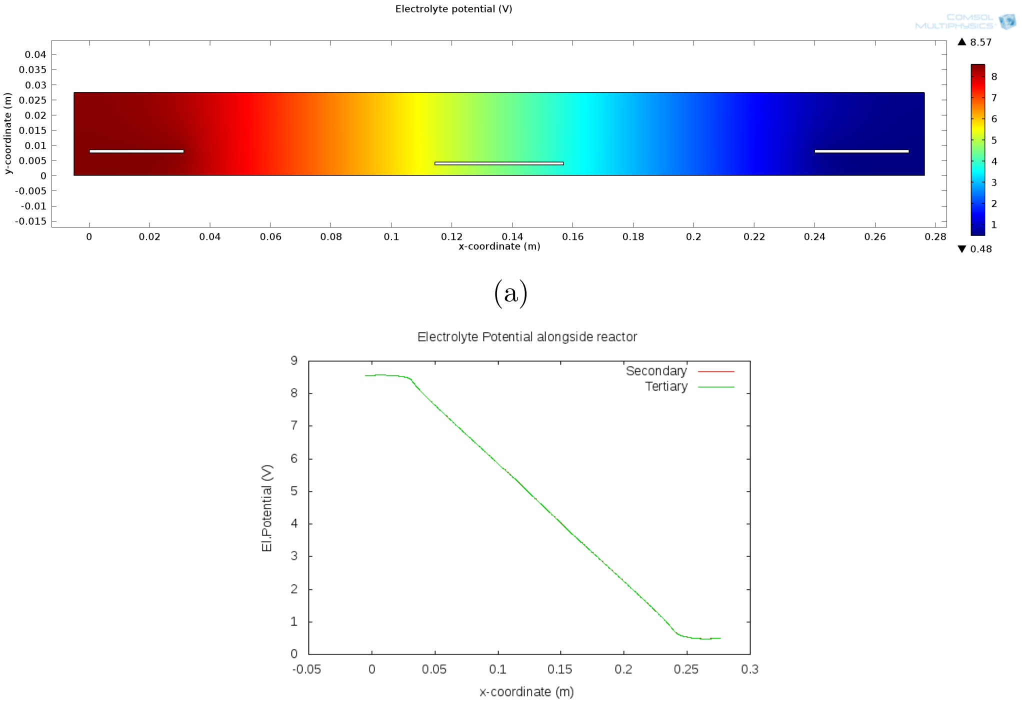

(a)

(b)

Figure 4.18: *Applied 10 V in Geometry III with Tertiary model:* ***a)*** *Electrolyte potential distribution in Tertiary model and* ***b)*** *Electrolyte potential along the reactor (at height of 0.006 m) for both Secondary and Tertiary models.*

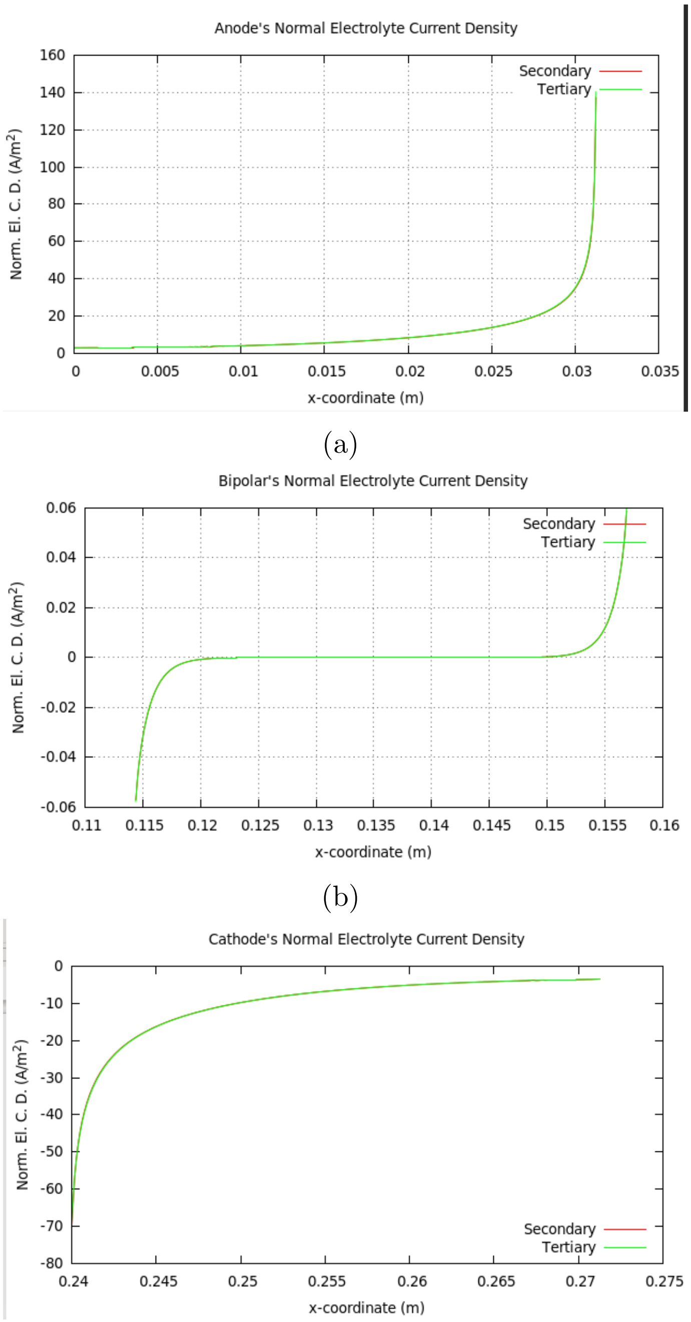

(a)

(b)

(c)

Figure 4.19: *Comparison of calculated normal electrolyte current density on the upper side of electrodes between Secondary and Tertiary models for applied* 10*V in Geometry I:* ***a)*** *Anode feeder electrode,* ***b)*** *Bipolar electrode and* ***c)*** *Cathode feeder electrode.*

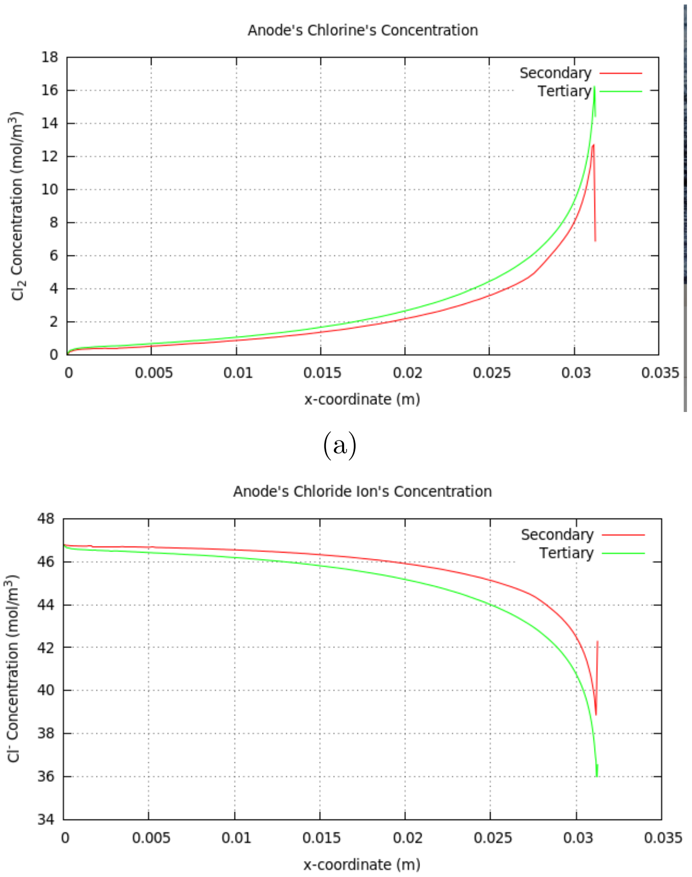

(a)

(b)

Figure 4.20: *Applied 10 V in Geometry I, anode's concentrations of* ***a)*** *Chlorine (Cl_2) and* ***b)*** *Chloride ion (Cl^-) are depicted between both Secondary and Tertiary model.*

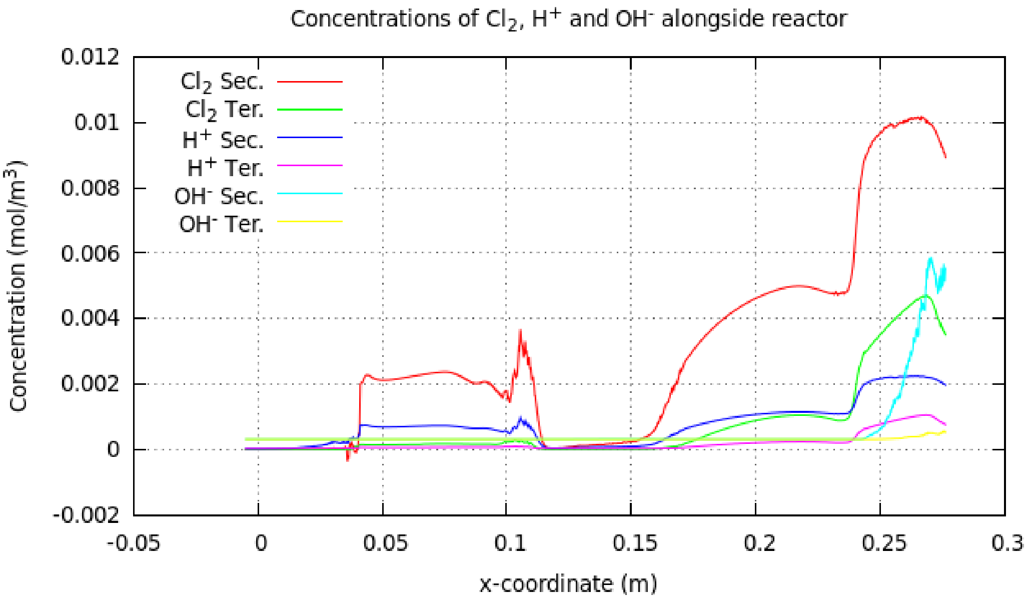

Figure 4.21: *Comparison of the concentration distribution, of the produced species* Cl_2*,* OH^- *and* H^+*, along the reactor (at height of 0.006 m) between the two models.*

be seen in Figure 4.22. There is only a region, in the vicinity of cathode, that the deviation can be considered significant but it is of order 10^{-3}. It is worth mentioning that this behavior is expected since the electroneutrality condition was forced for the inlet concentrations from the Secondary model.

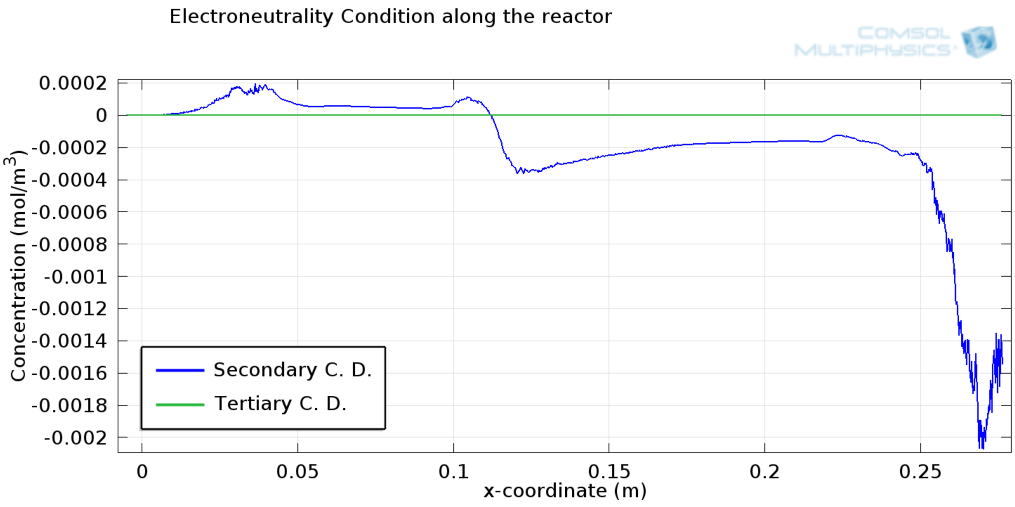

Figure 4.22: *Deviation from electroneutrality condition of the Secondary model.*

The Tertiary model calculates the electrolyte conductivity while the Secondary model assumes a constant value. Plotting the percentage error below 1% of the calculated Tertiary's electrolyte conductivity over the constant value of the Secondary model reveals regions, in the vicinity of the anode and the cathode (Figure 4.23). In the vicinity of the bipolar electrode, the calculated electrolyte conductivity by the Tertiary maintained constant value because under these operating conditions it behaves as an insulator producing no significant current values.

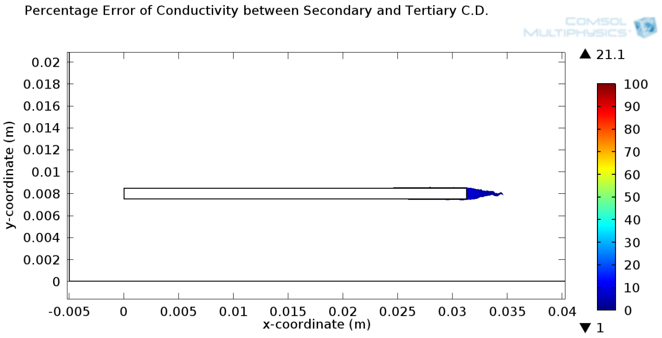

(a)

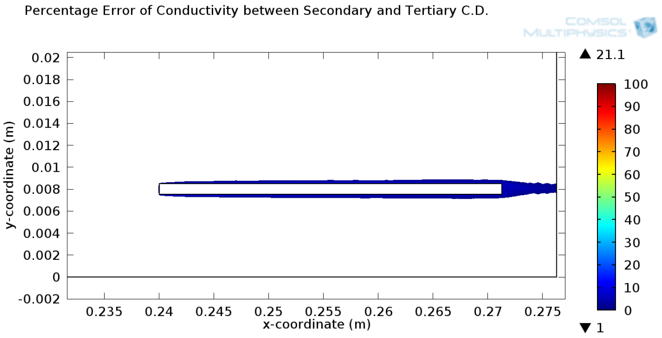

(b)

Figure 4.23: *Percentage error below 1% of the calculated Tertiary's electrolyte conductivity over the constant value of the Secondary model in the vicinity of* ***a)*** *anode and* ***b)*** *cathode.*

Even though the Secondary model, for the calculation of electrolyte current density, takes into account only the electrophoretic / migration term and assumes constant value for the electrolyte conductivity, it can predict reasonable results compared to a more complete model as that of Tertiary model (Figure 4.24).

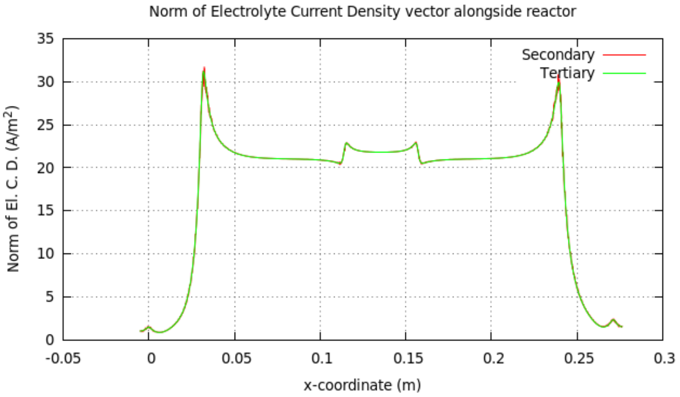

Figure 4.24: *Comparison of Norm Electrolyte current density, along the reactor (at height of 0.006 m), between the two models.*

4.5 Geometry I with Laminar and Turbulent Flow

In this section, we take into account the case with 30 V applied voltage as in section 4.1 and change laminar to turbulent flow (inlet velocity 1.5 m/s). Applying the mesh properties, as described in Table 4.3, the resulting mesh is identical to that of section 4.1 (69868 total elements with average element quality 0.914). The Laminar Flow module solves for 110490 degrees of freedom while Turbulent Flow module for 184150 DOFs.

The velocity magnitude distribution of the turbulent module is depicted in Figure 4.25

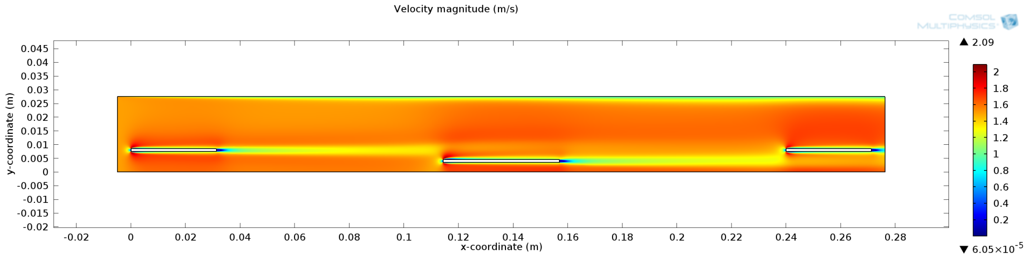

Figure 4.25: *Velocity magnitude distribution of Turbulent module.*

Due to the fact that the current case, with turbulent flow, is solved with the Secondary Current Distribution coupled with Transport of Diluted Species module, changes of variables will be made only where the velocity is present in the definition equations. The electrolyte potential distribution, in the Secondary model, is calculated via equation 3.36 where the convection term is not taken into consideration. Thus, the electrolyte potential and the norm electrolyte current density will be almost the same, independently of whether the flow is laminar or turbulent.

The above remark is confirmed in Figure 4.26. Also, the potential at the bipolar electrode is 15 V in both laminar (second case examined in section 4.1) and turbulent cases.

On the other hand, the velocity vector is present in the Nernst-Planck's flux of the species. So, due to the convective term of Nernst-Planck equation there will be differences in the concentration profile between the cases of laminar and turbulent flow. This is depicted in Figure 4.27 for the concentrations of produced species along the reactor (along the cut-line at height of 0.006 m).

Furthermore, there will be changes in concentration values of the species on the sides of the electrodes. In Figure 4.28, the concentrations of the

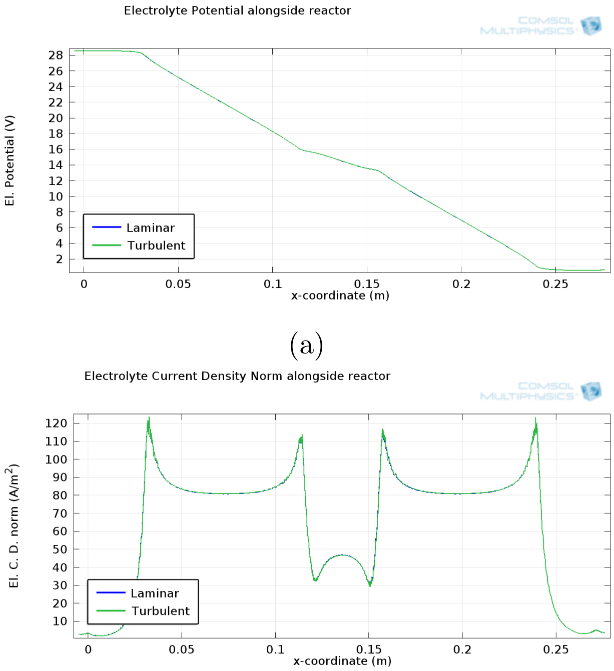

(a)

(b)

Figure 4.26: *Applied voltage 30 V in Geometry I, comparison of:* ***a)*** *Electrolyte potential distribution and* ***b)*** *Norm electrolyte current density between cases with laminar (inlet velocity 0.05m/s) and turbulent flow (inlet velocity 1.5 m/s).*

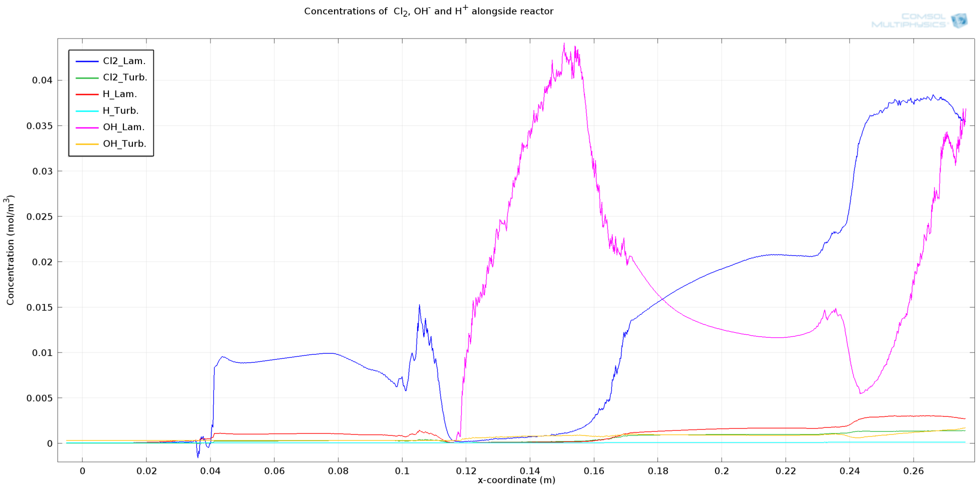

Figure 4.27: *Concentration distribution, of the produced species Cl_2, OH^- and H^+, along the reactor (at height of 0.006 m) between the cases of laminar (inlet velocity 0.05 m/s) and turbulent flow (inlet velocity 1.5 m/s).*

produced species (chlorine Cl_2 and hydrogen ion H^+) are shown on the anode and the bipolar electrode for the laminar and turbulent cases.

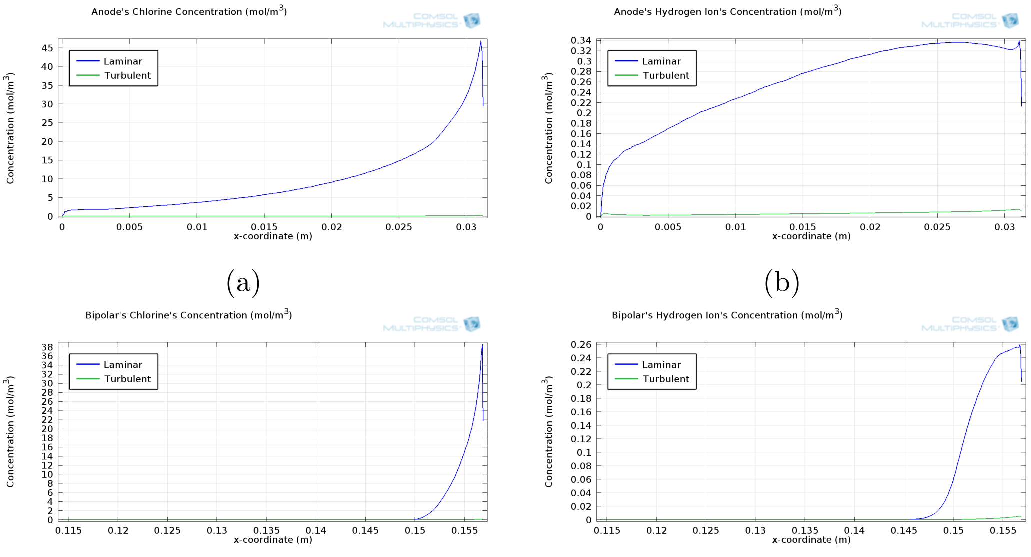

(a) (b)

(c) (d)

Figure 4.28: *Concentrations of the produced Chlorine Cl_2 and Hydrogen ion H^+ are shown on* ***a), b)*** *Anode feeder electrode and* ***c), d)*** *Bipolar electrode for the laminar (inlet velocity 0.05 m/s) and turbulent flow (inlet velocity 1.5 m/s).*

As a result of the changes in concentrations of chlorine Cl_2 and hydrogen ion H^+ (on anode and bipolar electrode), which affect the value of the produced current densities, changes in current density values of the reactions producing chlorine Cl_2 and hydrogen ion H^+ will occur. This can be seen in Figure 4.29.

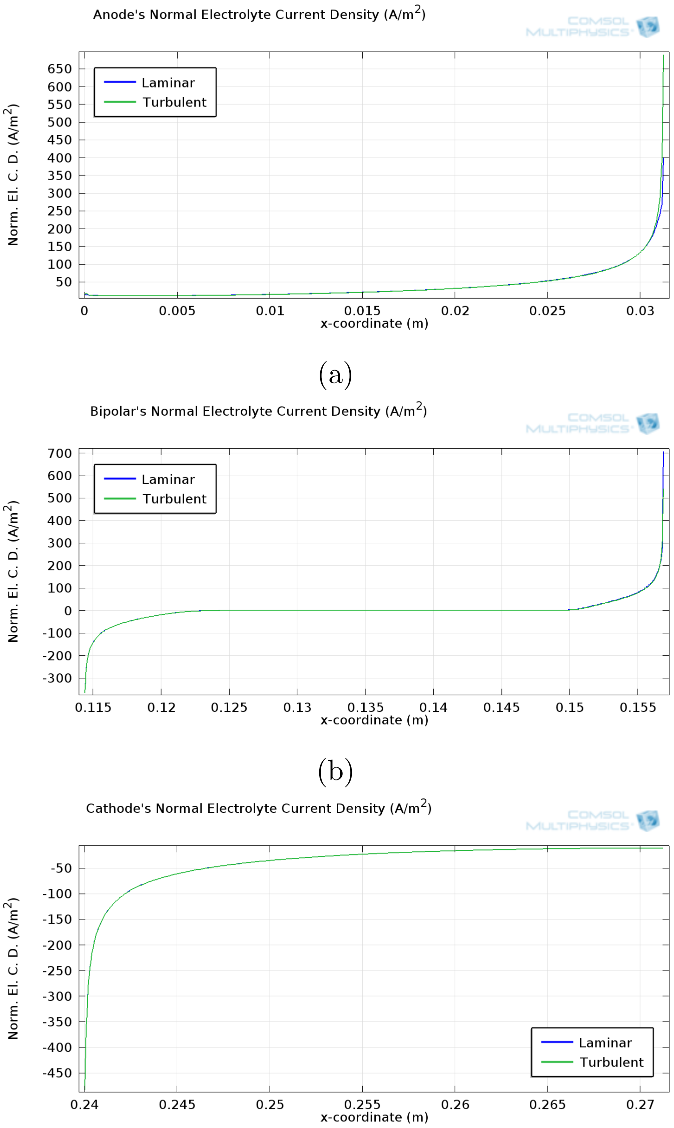

(a)

(b)

(c)

Figure 4.29: *Comparison of normal electrolyte current density between Laminar and Turbulent flow on the upper side of* ***a)*** *Anode feeder electrode,* ***b)*** *Bipolar electrode and* ***c)*** *Cathode feeder electrode.*

4.6 Geometry I with Reaction Rates in Homogeneous Phase

In this section, the effect of the reaction rates in the homogeneous phase (electrolyte) will be examined. The case of turbulent flow of section 4.5 will be considered as starting point where reaction rates the in homogeneous phase (electrolyte) will be introduced. In order to implement the reaction rates, two more variables will be added, the concentration of hypochlorous anion (OCl^-) and hypochlorous acid (HOCl).

Applying the mesh properties, as described in the beginning of the current chapter, the resulting mesh is identical to that of section 4.5 (69868 total elements with average element quality 0.914).

The addition of the two concentrations cause an increase of the number of degrees of freedom. Therefore, the Secondary module solves for 93899 (plus 6808 internal DOFs) degrees of freedom to 125109 (plus 9026 internal DOFs).

The Turbulent module is solved independently so the velocity distribution is identical to that of section 4.5.

The addition of reaction rates to the mass balance (Equation 3.42) does not affect the electrolyte potential distribution or the electrolyte current density as can be seen in Figure 4.30. Also, in Figure 4.30 the simulation produce overshoots that can be explained by the locally coarse mesh.

Furthermore, the normal electrolyte current density on the electrodes does not change, as shown in Figure 4.31.

Moreover, the dissociation of water (H_2O) and the dissociation of hypochlorous acid (HOCl) are considered fast reactions, so in steady state we assume that these reactions will approach the equilibrium point. This behavior can be seen in Figure 4.32, were the forward and backward reaction rates, for both reactions, are plotted. In Figure 4.33 the pH distribution is depicted.

Finally, the hydrolysis of chlorine (Cl_2) produces hypochlorous acid (HOCl) which is dissociated to hypochlorous anion (OCl^-). Thus, almost all chlorine is converted to hypochlorous acid and hypochlorous anion as shown in Figure 4.34 and 4.35.

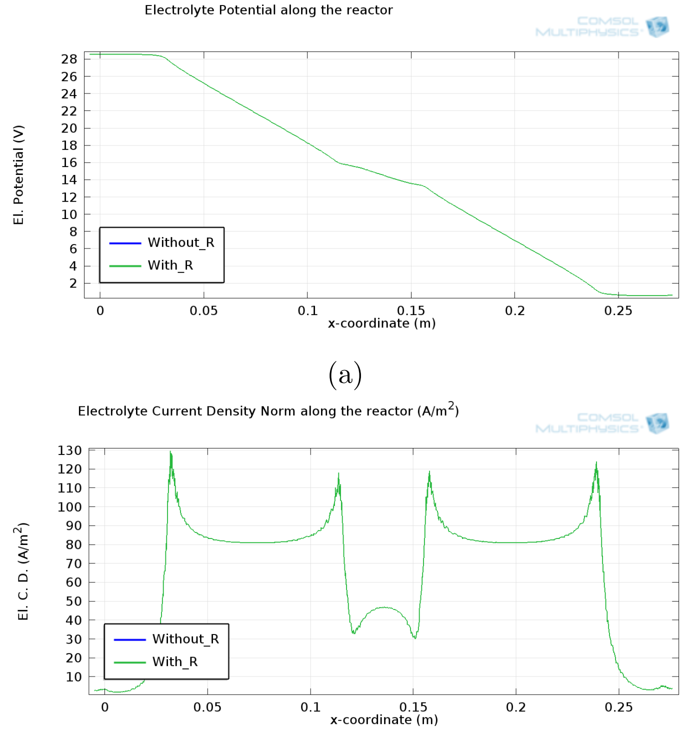

(a)

(b)

Figure 4.30: *Comparison of* ***a)*** *Electrolyte potential and* ***b)*** *Norm electrolyte current density between the case without and with reaction rates in homogeneous phase (electrolyte).*

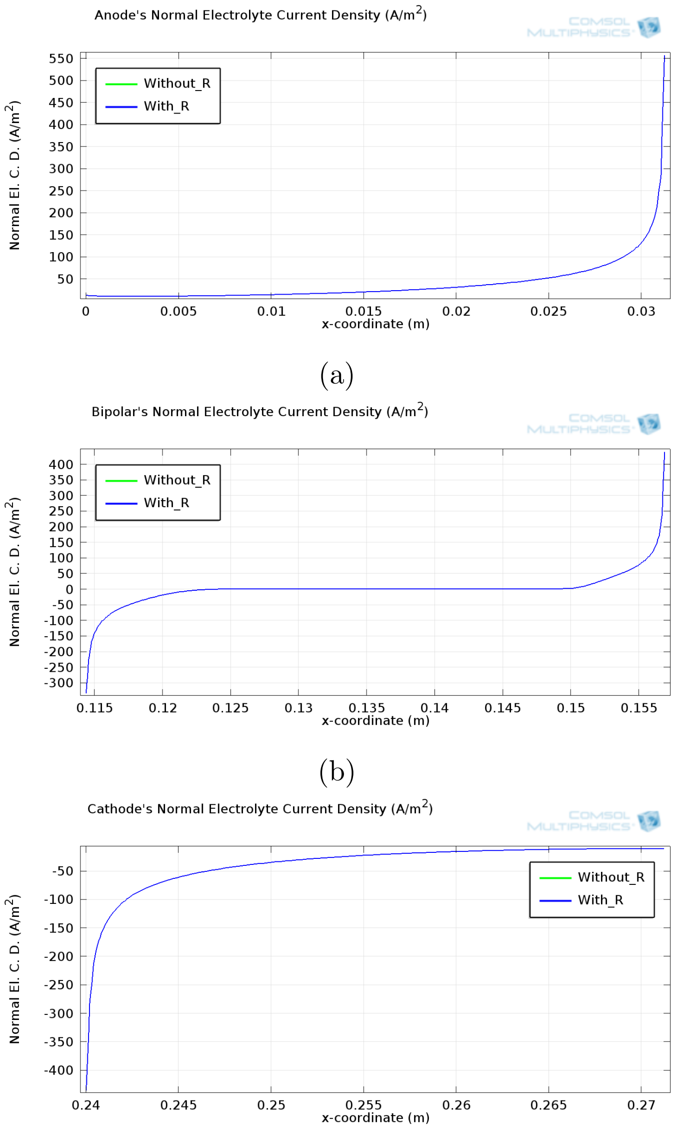

(a)

(b)

(c)

Figure 4.31: *Comparison of normal electrolyte current density between the cases without and with reaction rates in homogeneous phase (electrolyte) on the upper side of* ***a)*** *Anode feeder electrode,* ***b)*** *Bipolar electrode and* ***c)*** *Cathode feeder electrode.*

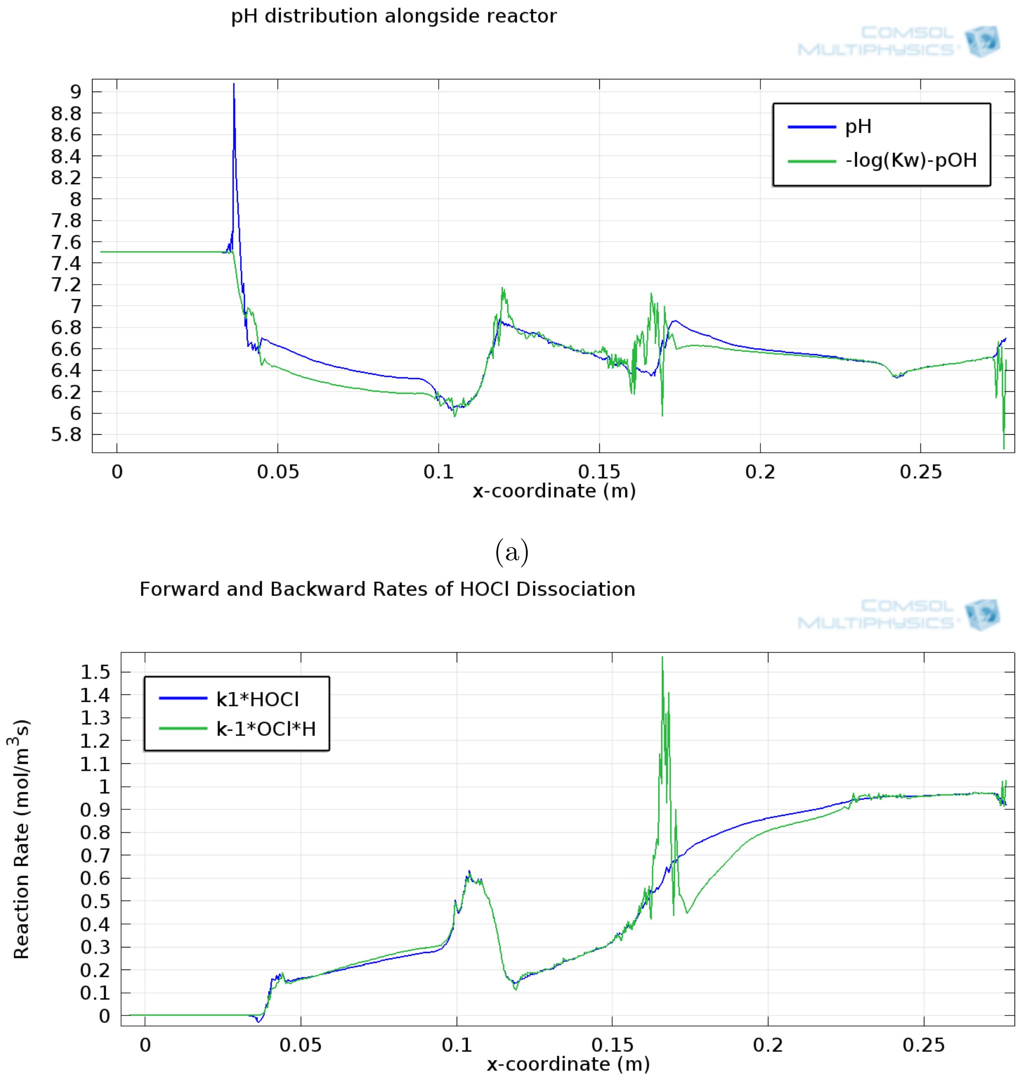

(a)

(b)

Figure 4.32: *Forward and backward rates of the* ***a)*** *Dissociation of water* (H_2O) *and* ***b)*** *Dissociation of hypochlorous acid (HOCl).*

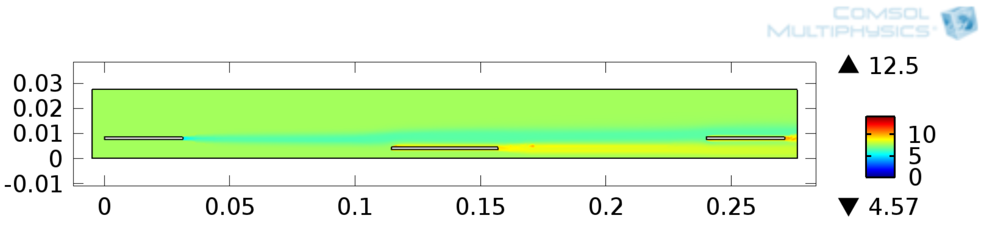

Figure 4.33: *Distribution of pH inside the reactor with Geometry I under implementation of reaction rates in the homogeneous phase of electrolyte.*

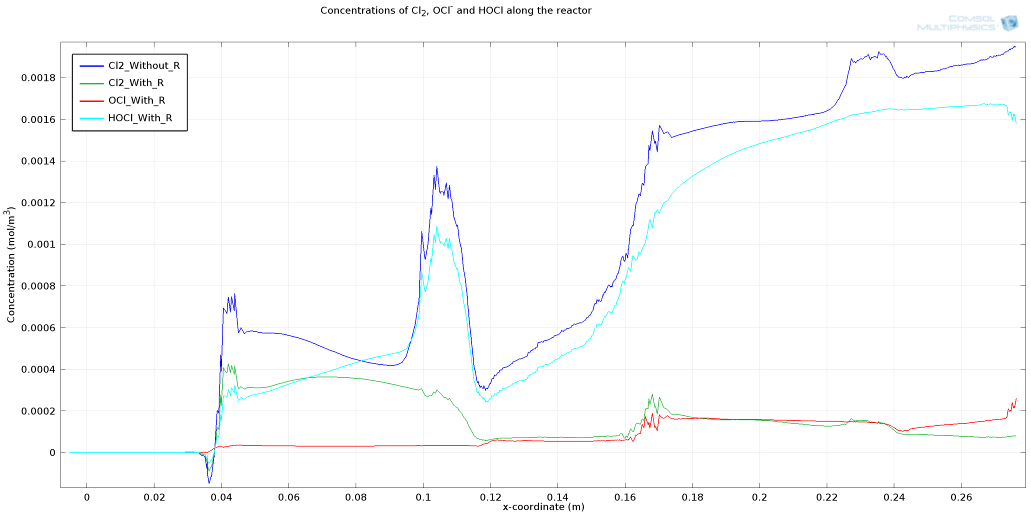

Figure 4.34: *Concentration of chlorine (Cl_2), hypochlorous acid (HOCl) and hypochlorous anion (OCl^-) along the reactor (at height of 0.006 m).*

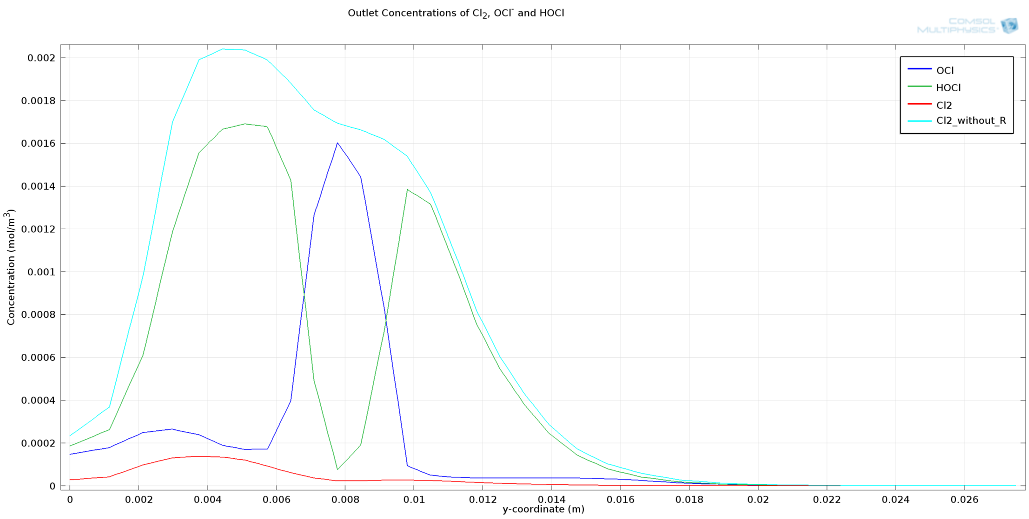

Figure 4.35: *Concentration of chlorine (Cl_2), hypochlorous acid (HOCl) and hypochlorous anion (OCl^-) at the outlet of the reactor.*

4.7 Complete Reactor

In this section a complete reactor with 2 anode electrodes, 3 cathode electrodes and 5 bipolar electrodes will be examined (Figure 4.36). For convenience, the bipolar electrode located on the top will be referred as first bipolar, the bipolar electrode which is located in the middle will be refereed as second and the bipolar on the bottom will be referred as third.

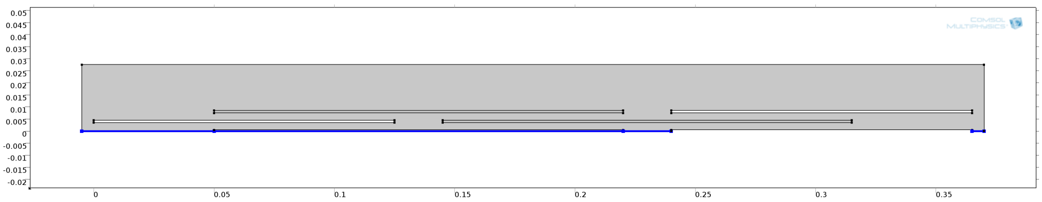

Figure 4.36: *Reactor with 2 anode feeder electrodes, 3 cathode feeder electrodes and 5 bipolar electrodes. Blue axis denotes symmetry plane.*

Applying mesh properties, described in Table 4.3, to this geometry leads to a computationally demanding case. Therefore, different mesh properties, have been chosen (Table 4.5). The resulting coarser mesh of the complete reactor consists of 159293 elements with average element quality 0.808. The Turbulent Flow, $k - \epsilon$ module solved for 454320 degrees of freedom. The inlet velocity is 1.5 m/s, so turbulent flow is considered (Figure4.37).

Even though different mechanistic scenarios predict apparent transfer

Table 4.5: *Mesh properties for the complete reactor.*

Mesh Properties	
Calibrate for	Fluid Dynamics, Fine
Boundaries	Extra Fine
Domain	Finer
Corner Refinement	0.25
Number of Boundary Layers	5

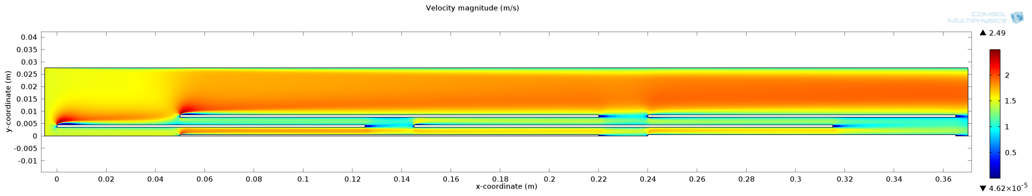

Figure 4.37: *Velocity magnitude distribution of the complete reactor.*

coefficients (or apparent symmetry factors) of value 1.5 and 0.5 (Equations 2.46 and 2.49), different coefficients has been observed experimentally. For the sake of completeness, an arbitrarily apparent transfer coefficient with value 1 is used,

$$i = i_0 e^{\frac{F}{RT}(E - E_{\mathrm{eq}})} \tag{4.2}$$

The coupling between Secondary Current Distribution module and Transport of Diluted Species module solved 552465 for degrees of freedom (plus 39152 internal DOFs). The applied voltage of the feeder electrodes is 30 V, thus implementing the Secondary Current Distribution module, the electrolytic potential distribution and the y-component electrolyte current density vector inside reactor are obtained (Figure 4.38).

As mentioned in section 4.3, the configuration of electrodes in geometry III resembles the configuration of electrodes inside the complete reactor. Thus, curves of local current density on bipolar electrodes are expected to be the same as those of geometry III. In Figure 4.39 the local current density of reactions producing Cl_2, O_2 and H_2 as well as the normal electrolyte current density are depicted, confirming the above remark.

Nevertheless, not all bipolar electrodes have the same behavior, as shown in Figure 4.42a. The first bipolar electrode is located above the anode electrode and above the second bipolar electrode, so on the lower side the local current density of the electrode reaction will be of similar form as in Figure 4.42a. Although, the upper side will have a different behavior as depicted in Figure 4.40a.

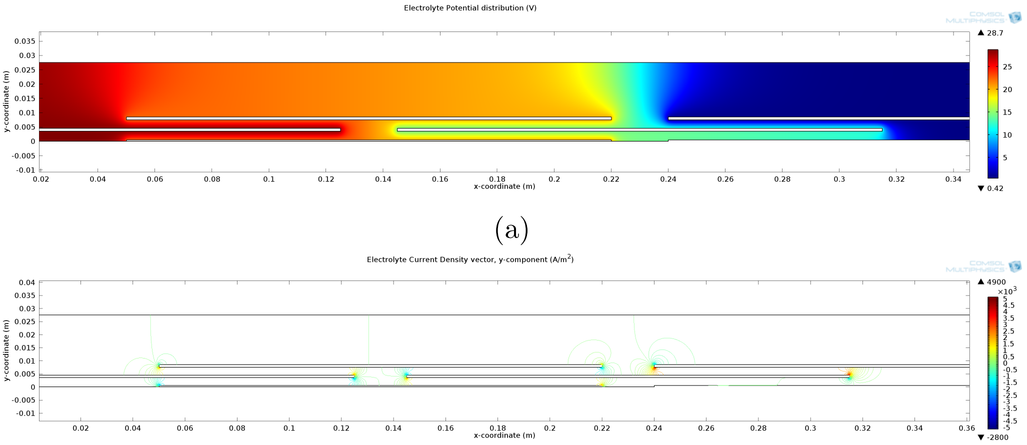

(a)

(b)

Figure 4.38: *Applied voltage 30 V in a full reactor with turbulent flow :* ***a)*** *Electrolyte potential distribution and* ***b)****Electrolyte current density vector, y-component.*

Moreover, under these operating conditions, Cl_2 evolution is the dominant reaction on the anode. The production of O_2 is much lower on all anodic parts of electrodes. Also, with this configuration, high chlorine concentration is produced. This, can be be seen in the outlet of the reactor (Figure 4.41).

Finally, in all cases of previous sections, the current produced by the Oxygen Evolution Reaction was of the form of Equation 2.49 with apparent transfer coefficient 0.5 resulting the chlorine evolution as the dominant reaction. In this section, the OER rate has been increased (lower Tafel) having transfer coefficient 1 but still chlorine evolution reaction is considered dominant. Thus, a question arises as to which reaction is dominant in the case of an even higher OER rate. Hence, assuming OER rate of the form of equation 2.46 (with apparent transfer coefficient 1.5) and focusing on the upper side of the third bipolar electrode, the local current density of the electrode reactions is plotted in Figure 4.42. This figure clearly shows that OER is the dominant reaction.

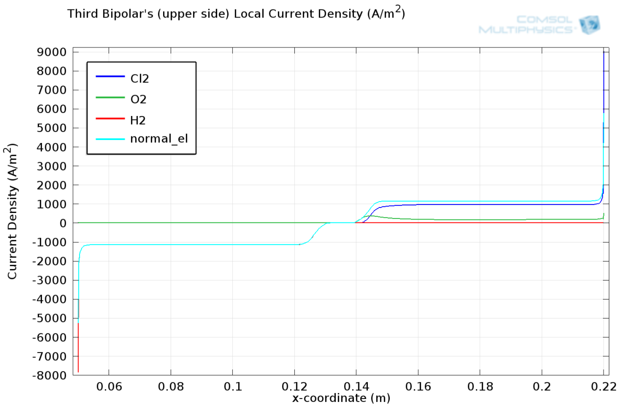

(a)

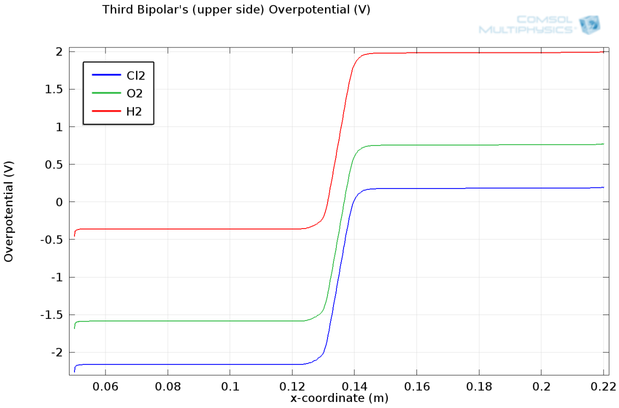

(b)

Figure 4.39: *Applied voltage 30 V in a complete reactor with turbulent flow on the upper horizontal side of the first bipolar electrode:* ***a)*** *Local current density of the reactions producing* Cl_2*,* O_2 *and* H_2 *also the normal vector of electrolyte current density is plotted. and* ***b)****Overpotential of the aforementioned reactions.*

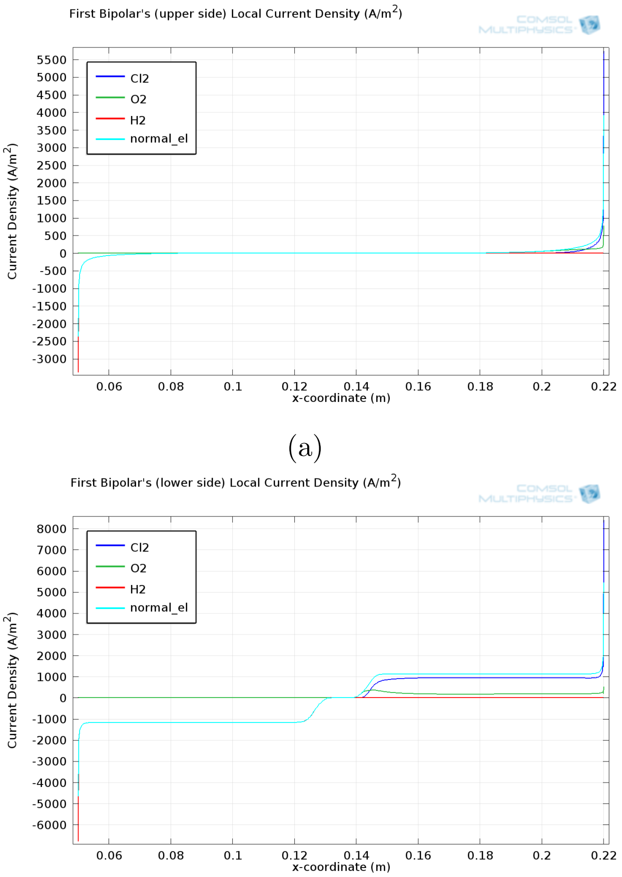

(a)

(b)

Figure 4.40: *Applied voltage 30 V in a complete reactor with turbulent flow, local current density of the reactions producing* Cl_2*,* O_2 *and* H_2 *also the normal vector of electrolyte current density is plotted on* ***a)*** *the upper horizontal side of the third bipolar electrode and* ***b)*** *the lower horizontal side of the third bipolar electrode.*

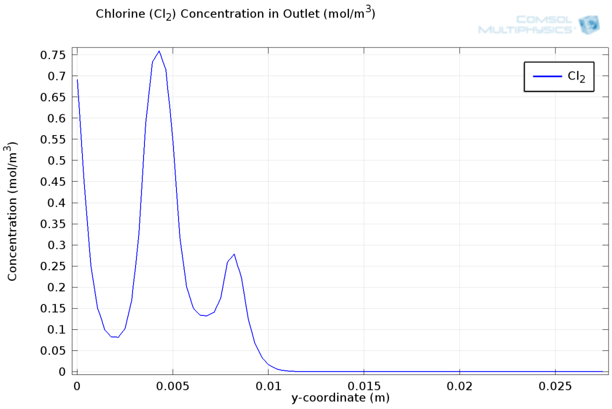

Figure 4.41: *Chlorine (Cl_2) concentration distribution at the outlet of the full reactor.*

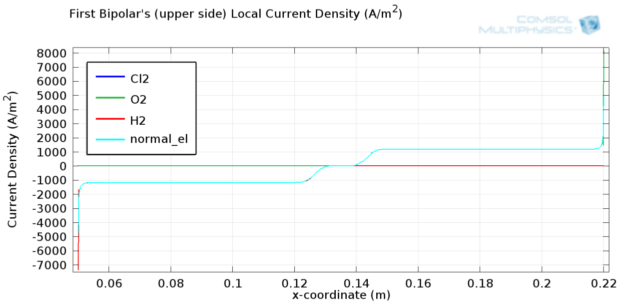

(a)

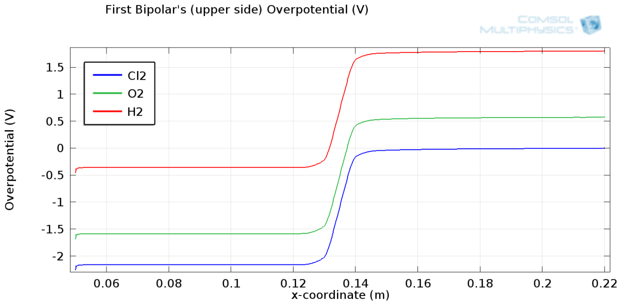

(b)

Figure 4.42: *Applied potential 30 V and OER with 1.5 apparent transfer coefficient in a complete reactor with turbulent flow on the upper horizontal side of the third bipolar electrode:* ***a)*** *Local current density of the reactions producing Cl_2, O_2 and H_2 (also the normal vector of electrolyte current density is plotted) and* ***b)*** *Overpotential of the aforementioned reactions.*

Chapter 5

Conclusions

The conclusions of the present work are summarized as follows:

- A realistic modeling of an electrochemical reactor of great technological importance has been achieved, based on the minimum assumptions. The COMSOL Multiphysics Software is appropriate for the modeling of complex electrochemical problems consisting of multiple electrochemical reactions, hydrodynamic flow, homogeneous chemical reactions and non trivial geometries.

- The optimum functioning of the bipolar electrodes is determined by the operational conditions and most importantly by the geometric characteristics of the reactor. An optimum geometry exists for which the chlorine production is maximized.

- The efficiency of chlorine production is crucially affected by the kinetics of the electrochemical reactions. More specifically, there is a competition between the production of oxygen and the production of chlorine. Nevertheless, for this specific application an adequate amount of chlorine is produced, under the operational conditions examined in this work.

- Since the competition between the OER and ClER is crucial, appropriate electrode materials capable of enhancing the kinetics of chlorine evolution and impede the oxygen evolution will promote the efficiency of the reactor.

- The comparison between Secondary and Tertiary Current Distribution models revealed that the differences of the results are not significant. Nevertheless, the Tertiary Current Distribution modeling is based on fewer assumptions thus the overall description is more realistic.

- Taking into account the reactions in the homogeneous phase results in a computationally demanding problem. On the other hand, the results are not affected significantly by the homogeneous chemical reactions. Thus satisfactory results can be obtained even if the homogeneous chemical reactions are ignored.

Appendix A

Multiple steps reaction rate

Let us consider a reaction of the form,

$$A \underset{k_b}{\overset{k_f}{\rightleftharpoons}} P \tag{A.1}$$

Let us assume that the above reaction occurs through three consecutive steps:

$$A \underset{k_{-1}}{\overset{k_1}{\rightleftharpoons}} X_1 \tag{A.2}$$

$$X_1 \underset{k_{-2}}{\overset{k_2}{\rightleftharpoons}} X_2 \tag{A.3}$$

$$X_2 \underset{k_{-3}}{\overset{k_3}{\rightleftharpoons}} P \tag{A.4}$$

Under *steady state* conditions and for stoichiometric numbers $v_i = 1$, the rate, v, of the overall reaction will be,

$$v = v_1 = v_2 = v_3 \tag{A.5}$$

where v_i are the rate of the corresponding step,

$$v_1 = k_1 C_A - k_{-1} C_{X_1} \tag{A.6}$$

$$v_2 = k_2 C_{X_1} - k_{-2} C_{X_2} \tag{A.7}$$

$$v_3 = k_3 C_{X_2} - k_{-3} C_P \tag{A.8}$$

Since $v_1 = v_2$ under *steady state* conditions, we obtain from Eq. A.6 and A.7,

$$k_1 C_A - k_{-1} C_{X_1} = k_2 C_{X_1} - k_{-2} C_{X_2} \tag{A.9}$$

thus, the concentration of X_1 can be written,

$$C_{X_1} = \frac{k_1}{k_2 + k_{-1}} C_A + \frac{k_{-2}}{k_2 + k_{-1}} C_{X_2} \tag{A.10}$$

Substituting Eq. 2.10 into Eq. A.6, a new expression for v_1 is obtained.

$$v_1 = \bar{k}_1 C_A - \bar{k}_{-1} C_{X_2} \tag{A.11}$$

where,

$$\begin{aligned} \bar{k}_1 &= \frac{k_1 k_2}{k_2 + k_{-1}} \\ \bar{k}_{-1} &= \frac{k_{-1} k_{-2}}{k_2 + k_{-1}} \end{aligned} \tag{A.12}$$

Now, since $v_1 = v_3$, from Eqs. (A.8) and (A.11) we obtain,

$$C_{X_2} = \frac{\bar{k}_1}{k_3 + \bar{k}_{-1}} C_A + \frac{\bar{k}_{-3}}{k_3 + \bar{k}_{-1}} C_P \tag{A.13}$$

The overall rate can be obtained be substituting Eq. A.13 in Eq. A.8, by taking into account that $v = v_3$.

$$v = \frac{k_3\bar{k}_1}{k_3 + \bar{k}_{-1}}C_A + \frac{k_{-3}\bar{k}_{-1}}{k_3 + \bar{k}_{-1}}C_P \tag{A.14}$$

But, the overall rate v is the algebraic sum of the forward and backward overall rates, i.e., $v = v_f - v_b$. Thus, from Eq. A.14, we can identify the overall forward rate,

$$v_f = \frac{k_3\bar{k}_1}{k_3 + \bar{k}_{-1}}C_A \tag{A.15}$$

and the overall backward rate,

$$v_b = \frac{k_{-3}\bar{k}_{-1}}{k_3 + \bar{k}_{-1}}C_P \tag{A.16}$$

Equation can be written,

$$\frac{1}{v_f} = \frac{1}{k_1 c_A} + \frac{k-1}{k_1 k_2 C_A} + \frac{k_{-1}k_{-2}}{k_1 k_2 k_3 C_a} \tag{A.17}$$

which is similar to Eq. 2.43 of Chapter 2. Finally, Equation A.16 can be written,

$$\frac{1}{v_b} = \frac{1}{k_3 C_P} + \frac{k_3}{k_{-3}k_{-2}C_P} + \frac{k_3 k_2}{k_{-3}k_{-2}k_{-1}C_P} \tag{A.18}$$

Bibliography

[1] URL: `http://www.comsol.com/model/download/184799/models.cfd.water_purification_reactor.pdf`.

[2] G. Bauer. *A Coupled Finite Element Approach for Electrochemical Systems*. Munich, Germany: PhD Thesis, 2012.

[3] J. O. Bockris. *Kinetics of Activation Controlled Consecutive Electrochemical Reactions: Anodic Evolution of Oxygen*. Volume 24, Number 4. Journal of Chemical Physics, 1955.

[4] J. O. Bockris. *J. Chem. Phys. 24, 817*. 1956.

[5] J. O. Bockris, B. Conway, and R. White. *Modern Aspects of Electrochemistry, No.14*. New York and London: Plenum Press, 1982.

[6] J. O. Bockris, A. Reddy, and M. Gamboa-Aldeco. *Modern Electrochemistry 2A: Fundamentals of Electrodics*. 2nd Edition. New York: Plenum Press, 1970.

[7] P. Byrne. *Mathematical modelling and experimental simulation of chlorate and chlor-alkali cells*. Ph.D. Thesis. Sweden: Stockholm University, 2001.

[8] P. Byrne et al. *A Simulation of the Tertiary Current Density Distribution from a Chlorate Cell*. 148, (10). Journal of The Electrochemical Society, 2001.

[9] C. Christiansen. 145th ed. Z. physik. Chern. B33, 1936.

[10] *Comsol, User's Guide*. Version 4.3. Heat Transfer Module, 2012.

[11] B. Conway et al. *Comprehensive Treatise of Electrochemistry*. Volume 7, Kinetics and Mechanisms of Electrode Processes. New York and London: Plenim Press, 1983.

[12] M. Deborde and U. von Gunten. *Reactions of chlorine with inorganic and organic compounds during water treatment—Kinetics and mechanisms: A critical review*. 13-51. Water Research 42, 2008.

[13] J. Duval, J. Leijn, and H. van Leeuwen. *Bipolar electrode behaviour of the aluminium surface in a lateral electric field.* 505, 1-11. Journal of Electroanalytical Chemistry, 2001.

[14] J. Duval et al. *Faradaic depolarization in the electrokinetics of the metal–electrolyte solution interface.* 260, 95–106. Journal of Colloid and Interface Science, 2003.

[15] J. Duval et al. *J. Phys. Chem. B , 107, 4143-4155.* 2003.

[16] J. Duval et al. *J. Phys. Chem. B , 107, 6782-6800.* 2003.

[17] J. Duval et al. *Rigorous Analysis of Reversible Faradaic Depolarization Processes in the Electrokinetics of the Metal/Electrolyte Solution Interface.* 107, 6782-6800. J. Phys. Chem. B, 2003.

[18] L. Gomez. *Preparation and Characterization of* $IrO_2 - RuO_2 - SnO_2$ *Ternary Mixtures fro Advanced Electrochemical Technology.* Phd Thesis. University of Ferrara, 2006.

[19] D. Hlushkou, R. Crooks, and U. Tallarek. *Numerical Simulation of Electric Field Gradient Focusing and Separation of Analytes in Microchannels with Embedded Bipolar Electrode.* High Performance Computing in Science and Engineering, 2009.

[20] S. Jin and S. Ye. *Oxygen Evolution on Titanium Anodes Coated with Conductive Metallic Oxides: Kinetics and Mechanism in Alkaline Solution.* pp.827-834. Electrochemica Acta, Vol. 41, No. 6, 1996.

[21] E. Lacasa et al. *Electrochemical disinfection of simulated ballast water on conductive diamond electrodes.* 516-523. Chemical Engineering Journal 223, 2013.

[22] M. Lyons et al. *The mechanism and kinetics of electrochemical water oxidation at oxidized metal and metal oxide electrodes. Part 1. General considerations: A mini review.* 60-62. Electrochemistry Communications 45, 2014.

[23] E. Mitha. *Numerical Modelling of Potential and Current Distributions in a Bipolar Electrolytic Cell.* Ph.D. thesis. France: École polytechnique fédérale de Lausanne, 1998.

[24] J. Morris. *The acid ionization constant of HOCl from* 5^oC *to* 35^oC. 3798–3805. J. Phys. Chem. 70, 1966.

[25] J. Newman and K. Thomas-Alyea. *Electrochemical Systems.* 3rd Edition. Wiley, 2004.

[26] N. T. Nguyen. *Micromixers:Fundamentals, Design, and Fabrication (Micro and Nano Technologies).* 1st Edition. William Andrew, 2008.

[27] B. Nielsen. *Control of Ballast Water Organisms with a Seawater Electrochlorination and Filtration System*. Master thesis. University of Washington, 2006.

[28] S. Payer and K. Neumann. 253rd ed. Chem. Exp. Didakt. 2, 1976.

[29] C. Ruiyong. *Electrochemical Chlorine Evolution at Sol-Gel Derived Mixed Oxide Electrocatalyst Coatings*. Saarland University, 2010.

[30] H. Santana and L. De Faria. *Oxygen and chlorine evolution on* $RuO_2 + TiO_2 + CeO_2 + Nb_2O_5$ *mixed oxide electrodes*. 3578-3585. Electrochemical Acta 51, 2006.

[31] Y. Tanaka. *Water dissociation in ion-exchange membrane electrodialysis*. 227-244. Journal of Membrane Science 203, 2002.

[32] Y. Tanaka. *Water dissociation in ion-exchange membrane electrodialysis*. 227-244. Journal of Membrane Science 203, 2002.

[33] A. Tseung et al. *Novel Acid-Resistant Oxygen Evolution Electrodes*. Luxembourg: Commission of the European Communities, 1989.

[34] C. Urgeghe. *Oxygen Evolution and Oxygen Reduction in Electrochemical Energy Conversion*. Phd Thesis. University of Ferrara, 2005.

[35] J. Vasconcelos and P. Boulos. *Characterization and Modeling of Chlorine Decay in Distribution Systems*. American Water Works Association, 1996.

[36] T. Wang and D. Margerum. *Kinetics of Reversible Chlorine Hydrolysis: Temperature Dependence and General-Acid/ Base-Assisted Mechanisms*. 33, 1050-1055. Inorg. Chem, 1994.

[37] D. Wilcox. *Turbulence Modeling for CFD*. California, USA: DCW Industries, Inc., 1993.